Kinetics and Catalysis, Vol. 43, No. 3, 2002, pp. 316–336. Translated from Kinetika i Kataliz, Vol. 43, No. 3, 2002, pp. 346–366.

Mathematical Modeling of Kinetics of Adenosine 5'-Triphosphate Hydrolysis Catalyzed by the Zn^{2+} Ion in the pH Range 7.4–8.3

E. Z. Utyanskaya*, B. V. Lidskii, and M. G. Neihaus****

** Emanuel Institute of Biochemical Physics, Russian Academy of Sciences, Moscow, 117977 Russia*

*** Semenov Institute of Chemical Physics, Russian Academy of Sciences, Moscow, 117977 Russia*

Received June 28, 2000

Abstract—Kinetic data on adenosine triphosphate (ATP) hydrolysis catalyzed by the Zn^{2+} ion in the pH range 7.4–8.3 are analyzed by the method of numerical simulation. The rates of forward and reverse reactions of isomeric conversion of the open conformation of $ZnATP^{2-}$ (Op), which is inactive in hydrolysis to ADP, to the active cyclic conformation $ZnATP^{2-}$ (Cy) in the specified range of pH are proportional to the concentration of H_3O^+ and characterized by the same rate constants as in the range of pH above 8.5. The mechanism of the isomeric conversion Op $\rightleftharpoons$ Cy involves the formation of a pentacovalent state at γ-P, pseudorotation, and the abstraction of OH^- from γ-P of the pentacovalent intermediate with the participation of H_3O^+ in a slow step. The sequence of steps for the formation and transformation of intermediates, which was established earlier for the $ZnATP^{2-}$ associates in the pH range 7.1–7.4, is applicable to this range of pH as well. In the analyzed range of pH, the contributions from the pH-independent channel of hydrolysis of the $ZnATP^{2-}$ associates and the pH-dependent channel of $CyOH^-$ and $Op(OH^-)_2$ species, which determine the formation of ADP and AMP at pH > 8.5, are comparable. Changes in the concentrations of intermediate products (monomeric and associates) in the course of hydrolysis are described. General base catalysis by a nitrogen base in the steps of formation of active centers for hydrolysis, the general acid catalysis of a coordinated water molecule, the exchange of medium OH^- with OH of γ-phosphate, the catalysis of conversion of the inactive conformation $ZnATP^{2-}$ to the active one by a proton, and a change of the rate-limiting stage of hydrolysis with a change in pH indicate the enzyme-like mechanism of the reaction.

INTRODUCTION

The study of adenosine triphosphate (ATP) hydrolysis catalyzed by the Zn^{2+} ion [1–5] allowed us to conclude that atom N7 of the adenine base of the ATP^{4-} molecule coordinated to Zn^{2+} in the cyclic conformation of the monomeric molecule directs the attack of OH^- on the phosphoric atom of $ZnATP^{2-}$ leading to the selective formation of ADP + P_i (where P_i is the inorganic phosphate). In our previous studies [1, 2], we considered a structural model of reaction center for hydrolysis in which the active ion $M^{2+}OH^-$ is opposite to the cleaved P_γ–OP_β bond with M^{2+} bound to atom N7 of its own adenine base and the O^- atom of its own γ-phosphate group. We have shown that the $Zn^{2+}OH^-$ ion is active in hydrolysis to ADP + P_i only in the cyclic conformation of the phosphate chain both in the $ZnATP^{2-}OH^-(CyOH^-)$ monomer and dimer $(ZnATP^{2-})_2H^+OH^-$ [1–6]. The assumed structures of the cyclic (Cy) monomeric $ZnATP^{2-}$ species, open (Op) monomeric $ZnATP^{2-}$ species, and a dimeric complex (D) formed by two monomeric cycle molecules are shown in Fig. 1 in [9], and the structure of the dimeric complex is shown in Scheme 1. The hydrogen bond between the coordinated water molecule and γ-phosphate becomes stronger than under the conditions of hydration in the absence of M^{2+} [7]. When a proton is abstracted from the coordinated water molecule of Cy, the hydrogen bond of the $Zn^{2+}OH^-$ with O^- ions of the terminal phosphate breaks. The open monomeric form $ZnATP^{2-}$ is believed to be a β,γ-conformer [8]. The hydrolysis of the dimeric associate determines the kinetics of the pH-independent channel [4, 5], whereas the hydrolysis of the monomeric $CyOH^-$ determines the kinetics of the pH-dependent channel [5, 6]. Recently, we published a detailed analysis (using the method of numerical simulations) of ATP hydrolysis catalyzed by the Zn^{2+} ion at pH 8.5–9.0 [9]. We considered the mechanism for the isomeric conversion of the open ($Op–Zn^{2+}$ is only bound to the phosphate chain) and cyclic conformations of the $ZnATP^{2-}$ complexes, which are active in hydrolysis to ADP (Scheme 1 in [9]). Equilibrium in step 6 (the formation of the open monomeric $Op(OH^-)_2$ species in which OH^- substitutes for N7 in the coordination sphere of Zn^{2+} in $CyOH^-$) is established much faster then filling Cy up from Op in step 5

0023-1584/02/4303-0316$27.00 © 2002 MAIK "Nauka / Interperiodica"

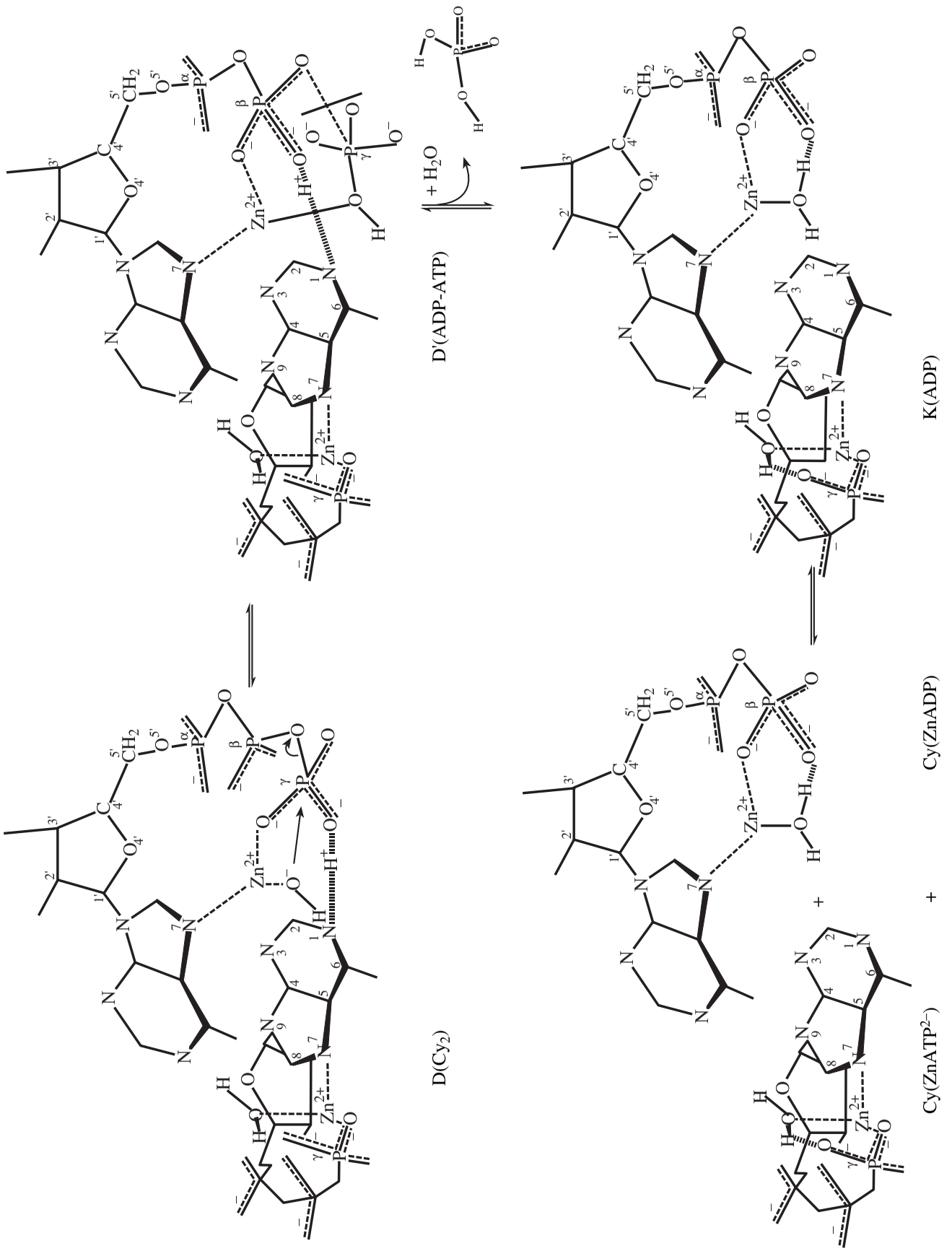

Scheme 1

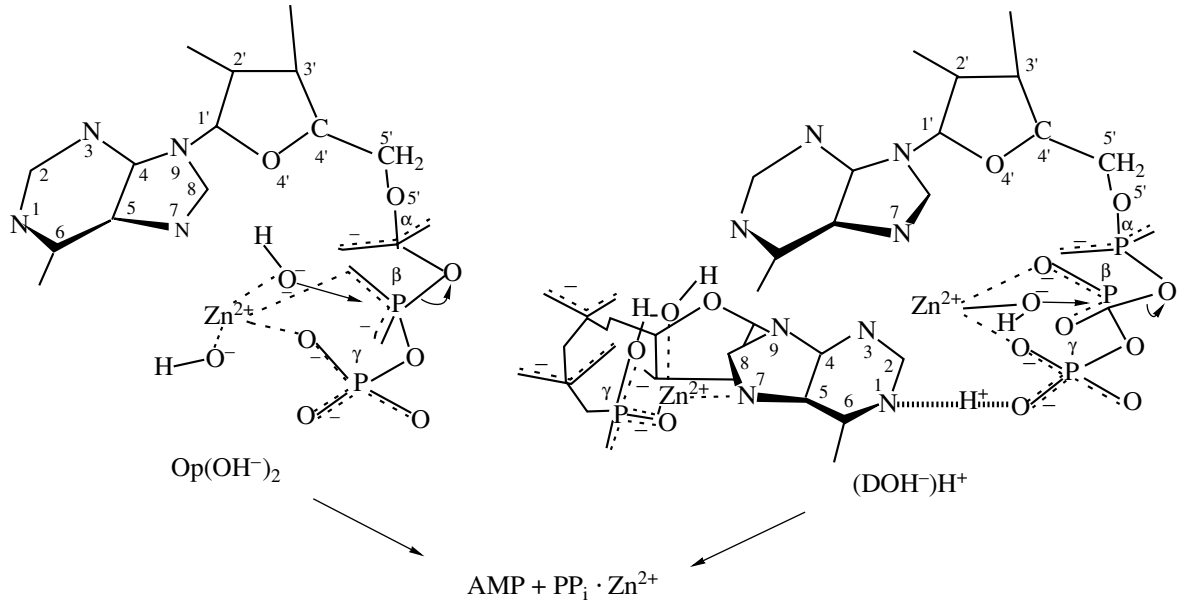

Scheme 2

and violates the equilibrium ratio $([Op]/[Cy])_0 \approx 2.6$, which is characteristic of lower pH values [10–13]. This violation takes place at the initial stage of hydrolysis at pH > 8.5. We found that the slow formation of Cy from Op and the disturbance of the isomeric equilibrium occurs at pH > 8.2 and is catalyzed by the H_3O^+ ion, as we conjectured earlier (Scheme 1 in [9]). The slow cleavage of the P_γ–OP_β bond at the initial stage of hydrolysis is rate-limiting at pH 7.1–8.2, whereas the rate of Op $\rightleftharpoons$ Cy isomeric conversion is comparable or even lower than the rate of bond dissociation at pH > 8.5 [6, 9]. The formation of Cy in step 5 (Scheme 1 in [9]) limits the accumulation of the final products (ADP and AMP) at pH > 8.5, and both products are formed via parallel pathways from the beginning of reaction [5, 6]. In addition to slow step 5 at pH > 8.5, a direct slow isomeric conversion $CyOH^- \rightleftharpoons OpOH^-$ occurs. These ions are formed by the protolysis of water in Cy and $Op(ZnATP^{2-} \cdot OH_2)$. This transformation occurs via the pentacovalent intermediates $Cy'OH^-$ and $Op'OH^-$ (steps 10 and 11), in which OH^- from the medium is added to the γ-phosphate groups of the monomeric species and OH^- at Zn^{2+} is liberated to the medium (Scheme 1a in [9]). The rate-limiting step in the ion isomeric conversion is pseudorotation (step 7). Both isomeric conversion processes (steps 5 and 7 of Scheme 1 in [9]) determine a drastic decrease in the rate in the course of the process at pH > 8.5. The initial drastic decrease in the rate is sensitive to the rate constants of step 7, whereas the description of the end portion of the kinetic curve (with a slowly changing rate) is sensitive to both the rate constants of step 7 and to filling Cy up from Op in step 5 [9].

In our earlier paper [14], we proposed the whole sequence of steps for the formation and transformation of intermediates over a broad interval of concentrations (4×10^{-4}–3×10^{-1} mol/l) at pH 7.1–7.4. In this pH range, the pH-independent channel of $ZnATP^{2-}$ associate hydrolysis dominates. The rates and equilibria of active center formation in the pH-independent channel (step 9 of Scheme 2 [9]) are determined by proton transfer from a coordinated water molecule to γ-phosphate with the formation of a hydrogen bond between atom N1 of the second $ZnATP^{2-}$ molecule, which functions as the general base catalyst, and the γ-phosphate group of the first $ZnATP^{2-}$ molecule (Scheme 1). Analysis of Scheme 2 was carried out in [9] assuming fast proton transfer in step 9 and equilibrium established between the open (Σ[Op]) $ZnATP^{2-}$ species (Op, Op', and O", see [9, 14]), $Cy(ZnATP^{2-})$, and dimer (D) in the initial step of hydrolysis. In the pH-independent channel of the dimer hydrolysis, AMP is also formed. This reaction occurs via steps 14 and 15 in parallel with the formation of ADP in the sequence of steps 2 $\longrightarrow$ 16 $\longrightarrow$ 17. AMP is formed from the intermediate product $(DOH^-)H^+$ (Scheme 2). It is formed from D by the substitution of the OH^- ion bound to Zn^{2+} situated opposite to the γ-phosphate group by another OH^- bound to Zn^{2+} situated opposite to the β-phosphate group (step 14). Then, $(DOH^-)H^+$ slowly decomposes in step 15 into AMP + pyrophosphate (PP_1), and regenerates the $Cy(ZnATP^{2-})$ molecule. The dimeric model adequately described kinetics at pH 7.1–7.4 at the initial concentration $[Zn \cdot ATP]_0 = 7.2 \times 10^{-3}$–$2.74 \times 10^{-1}$ mol/l, and the same model was incorrect for experiments carried out at $[Zn \cdot ATP]_0 = 4 \times 10^{-4}$ mol/l. Calculations showed that dimer D is formed much more slowly at low concentrations than at high concentrations [14]. Scheme 3, which

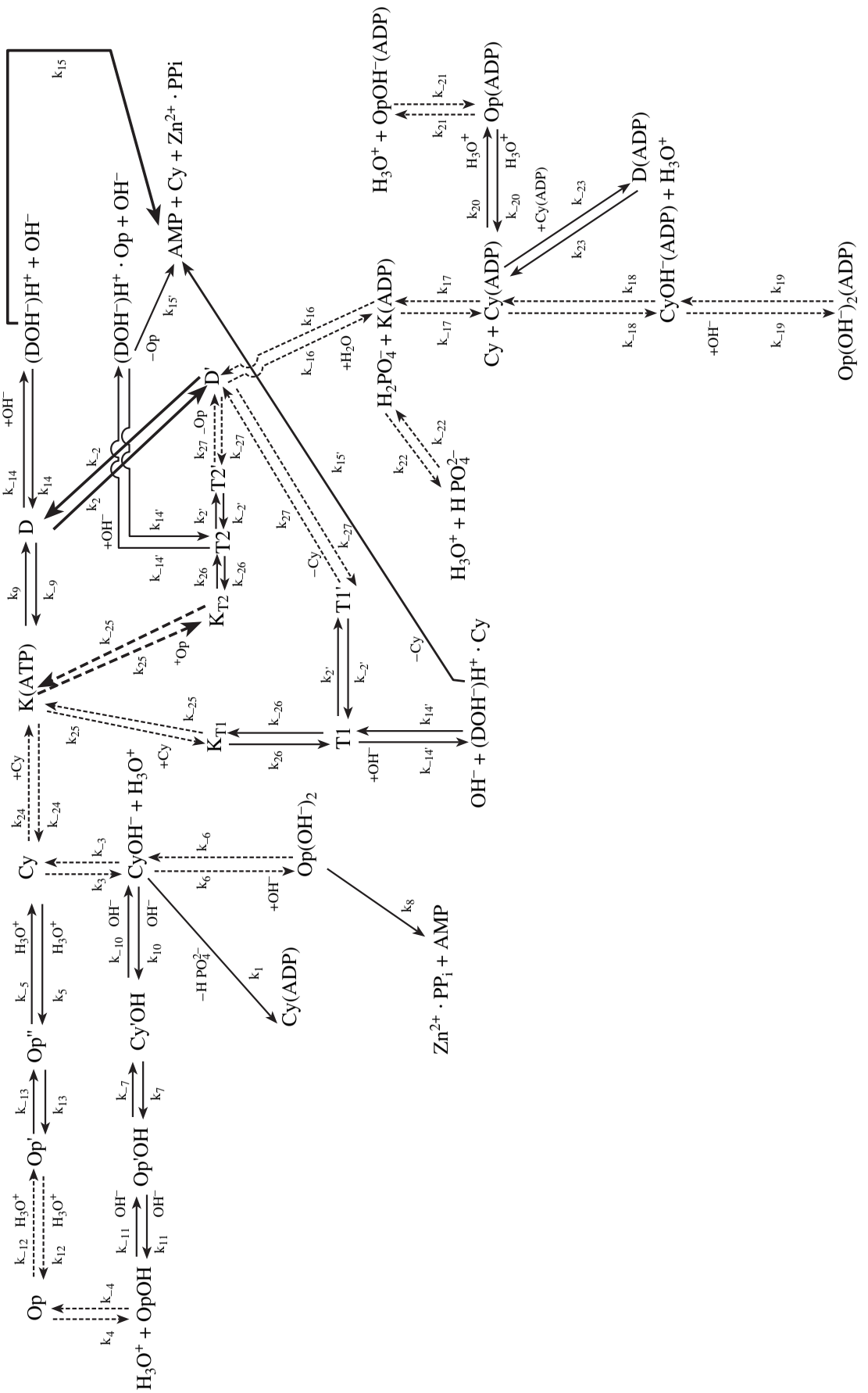
AMP + Cy + Zn2+ · PPi
(DOH−)H+ + OH−
(DOH−)H+ · Op + OH−
H3O+ + OpOH−(ADP)
Op(ADP)
D(ADP)
CyOH−(ADP) + H3O+
Op(OH−)2(ADP)
H2PO4− + K(ADP)
Cy + Cy(ADP)
H3O+ + H PO4 2−
OH− + (DOH−)H+ · Cy
K(ATP)
D
D'
T2
T2'
KT2
T1'
KT1
T1
Op(OH−)2
CyOH− + H3O+
Cy
Op"
Op'
Op'OH
Cy'OH
Op
H3O+ + OpOH
Cy(ADP)
Zn2+ · PP1 + AMP

Scheme 3

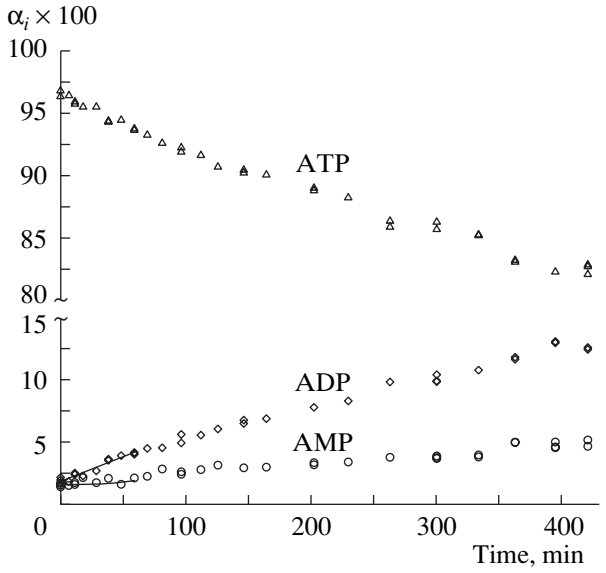

Fig. 1. Kinetic curves of ATP consumption and ADP and AMP formation at pH = 8.05. $[Zn \cdot ATP]_0 = 2.75 \times 10^{-3}$ mol/l; $[NaClO_4] = 0.128$ mol/l; 50°C.

takes into account the role of trimeric associates $ZnATP^{2-}$ in the formation of species that are active in hydrolysis, allowed us to describe the complete set of experimental data on the concentration dependence of hydrolysis kinetics at pH 7.1–7.4. Scheme 3 assumes that, at the initial stage of hydrolysis, the dimeric complexes of two Cy molecules (K(ATP)), as well as trimeric associates in which the third $ZnATP^{2-}$ molecule in Cy or Op species is attached by the stacking-interaction (the third molecule has the Cy species in K_{T1} and the Op species in K_{T2}), are formed at higher rates. Dimers D and trimers T1 and T2 are formed from K_{T1}, K_{T2}, and K(ATP) complexes by proton transfer from the coordinated water molecule with the formation of a hydrogen bond between N1 of the second Cy molecule and γ-phosphate of the first Cy molecule. Further pathways for the transformations of dimers and trimers in slow steps are similar and result in the formation of D' and T1' or T2' (steps 2 and 2' are the proton transfer to β-phosphate). Trimers also substitute the OH^- ion at Zn^{2+} like dimers with the formation of $(DOH^-)H^+ \cdot Cy$ (or Op) complexes, which further lose Cy (or Op) in a slow step to yield $AMP + Cy + Zn^{2+} \cdot PP_i$. The rate and equilibrium constants of the main steps were estimated in [9, 14]. At pH > 8.8, the calculations according to the trimeric and dimeric models give close results because the kinetics is largely determined by the monomeric species [9].

In this paper, we present the results of the numerical simulation of the kinetics of Zn · ATP (1 : 1) hydrolysis in the range of pH that is intermediate between pH > 8.5, at which the main role belongs to monomeric intermediates ($CyOH^-$ and $Op(OH^-)_2$), and the pH at which the $ZnATP^{2-}$ associates dominate. The contributions of both channels at pH 7.4–8.3 are comparable. Analysis of kinetics in the indicated intermediate range of pH makes it possible to estimate the applicability of the whole scheme of consecutive transformations of intermediates proposed in [14]. The rate constants of step 5 were earlier determined at pH 8.7–9.0, where kinetic curves are most sensitive to their changes. The rates of both reactions of conformer transformation (forward and reverse) in the specified range were proportional to $[H_3O^+]$. In this work, we present data that show that the kinetic equation for step 5, which limits the isomeric conversion Op $\rightleftharpoons$ Cy, is applicable over the whole range of pH 7.6–9.0.

RESULTS AND DISCUSSION

We analyze hydrolysis kinetics at pH 7.4–8.3 in three series of experiments carried out at three constant values of $[Zn \cdot ATP]_0$ (Table 1): $[Zn \cdot ATP]_0 = (2.74 \pm 0.05) \times 10^{-3}$ mol/l in series I; $[Zn \cdot ATP]_0 = (4.20 \pm 0.07) \times 10^{-3}$ mol/l in series II; and $[Zn \cdot ATP]_0 = (0.401 \pm 0.001) \times 10^{-3}$ mol/l in series III. Kinetic experiments were carried out at 50°C and a given value of pH, which was maintained constant by adding the solution of NaOH of the known concentration. The experimental procedure, the method of product analysis carried out by ion-pair reverse phase high-performance liquid chromatography on a C-18 stationary phase (Separon SGX C-18), as well as the methods for computational experiments, were described in detail in our previous publications [5, 9, 14, 16]. Figure 1 shows the kinetic curves for the consumption of ATP and the formation of ADP and AMP for a run carried out at pH 8.05 (run 5, Table 1). Kinetic curves of this form are typical of pH 7.4–8.3. At the initial stage of hydrolysis, the molar fraction of ATP decreases, whereas the molar fraction of ADP increases. The initial decrease in the rate of ADP formation is not as pronounced as at pH > 8.5. The rates of ATP consumption and ADP formation steadily decrease in the course of the process. The formation of AMP in all runs begins after an induction period, which shortens with an increase in pH at a constant concentration of Zn · ATP and with an increase in $[Zn \cdot ATP]_0$ at a constant pH value (Table 1). In series III with a low initial concentration of Zn · ATP, the initial rate of ADP formation determined by the transformation of monomeric $CyOH^-$ increases with an increase in pH. In series I (runs 1–11), the initial rate of ADP formation changes slightly below pH ≈ 8 within the experimental scatter and then increases with an increase in pH [5].

Consideration of the pH-Independent Hydrolysis Channel in the Framework of the Dimeric Model

Figure 2 shows experimental kinetic curves for the formation of ADP calculated according to scheme 2 (curves *1*) in the framework of the dimeric model for runs 1 (Fig. 2a) and 12 (Fig. 2b) carried out at a pH

Table 1. Experimental conditions at pH 7.4–8.3

Series	Run	pH*	$[NuP]_0 \times 10^3$, mol/l	$[Zn^{2+}] \times 10^3$, mol/l	$[NaClO_4]$, mol/l	$[Zn \cdot ATP]_0 \times 10^3$, mol/l	$[ZnATP^{2-}]_0 \times 10^3$, mol/l	$w_{0,\,ADP} \times 10^6$, mol l^{-1} min^{-1}	$\tau_{ind,\,AMP}$, min
I	1	7.45 ± 0.04	2.89	2.88	0.108	2.79	2.48	0.809 ± 0.087	≈60
	2	7.53 ± 0.04	2.90	2.90	0.110	2.79	2.49	1.08 ± 0.08	≈60
	3	7.84 ± 0.06	2.89	2.82	0.109	2.76	2.36	0.801 ± 0.052	≈60
	4	8.00 ± 0.05	2.73	2.61	0.100	2.61	2.18	0.980 ± 0.183	≈40
	5	8.05 ± 0.04	2.87	2.75	0.128	2.75	2.29	1.12 ± 0.19	≈45
	6	8.10 ± 0.03	2.84	2.81	0.108	2.74	2.24	0.960 ± 0.060	≈40
	7	8.14 ± 0.04	2.87	2.75	0.128	2.75	2.20	0.950 ± 0.060	≈40
	8	8.21 ± 0.04	2.88	2.80	0.097	2.74	2.15	0.987 ± 0.175	≈25
	9	8.24 ± 0.02	2.87	2.81	0.108	2.77	2.12	1.17 ± 0.16	≈15
	10	8.34 ± 0.03	2.87	2.80	0.107	2.75	2.03	1.24 ± 0.08	≈20
	11	8.50 ± 0.02****	2.87	2.74	0.110	2.70	1.89	(2.8**)0.916 ± 0.155***	8
II	12	7.47 ± 0.04	4.48	4.23	0.106	4.23	3.77	1.75 ± 0.13	≈40
	13	7.48 ± 0.05	4.51	4.04	0.126	4.04	3.60	1.71 ± 0.19	≈30
	14	7.62 ± 0.04	4.47	4.23	0.121	4.23	3.72	1.64 ± 0.36	≈35
	15	7.82 ± 0.04	4.47	4.23	0.102	4.23	3.62	2.23 ± 0.17	≈30
	16	7.90 ± 0.03	4.47	4.23	0.150	4.23	3.56	2.27 ± 0.32	≈35
	17	8.00 ± 0.03	4.48	4.14	0.106	4.14	3.45	1.87 ± 0.12	≈25
	18	8.03 ± 0.02	4.46	4.22	0.150	4.22	3.52	2.37 ± 0.37	≈20
	19	8.13 ± 0.03	4.47	4.23	0.099	4.23	3.47	2.91 ± 0.72	≈20
	20	8.20 ± 0.02	4.44	4.25	0.122	4.25	3.33	2.59 ± 0.58	≈15
III	21	7.15 ± 0.05****	0.421	0.402	0.113	0.402	0.362	0.0172 ± 0.0016	≈360
	22	7.66 ± 0.03	0.420	0.401	0.111	0.401	0.352	0.0380 ± 0.0074	≈260
	23	7.81 ± 0.04	0.421	0.402	0.111	0.402	0.344	0.0278 ± 0.0033	≈150
	24	8.00 ± 0.03	0.419	0.400	0.110	0.400	0.333	0.0411 ± 0.0033	≈40
	25	8.19 ± 0.04	0.419	0.400	0.110	0.400	0.314	0.0664 ± 0.0040	≈10

Note: $[NuP]_0$ is the total initial concentration of nucleoside-5-phosphates; $[NaClO_4]$ is the $NaClO_4$ concentration in a cell; the initial concentration of $ZnATP^{2-}$ species: $[ZnATP^{2-}]_0 = a[Zn \cdot ATP]_0$, where a is the molar fraction of $ZnATP^{2-}$ in the balance of species at a given value of pH (using the results of potentiometric titration [15]); $Zn \cdot ATP$ means that Zn^{2+} is in the solution with an equal equivalent of ATP without specifying species present. $w_{0,\,ADP}$ is the initial rate of ADP formation (calculated from the kinetic curve of an increase in the ADP concentration). The intervals of errors of the initial rates are indicated for 95% probability.

* The average value of pH in the experiment and the accuracy with which it is kept constant.

** The rate of ADP formation before the induction of AMP formation.

*** The rate of ADP formation after the induction period of AMP formation.

**** Analyzed experiment carried out at pH < 7.4 and >8.3.

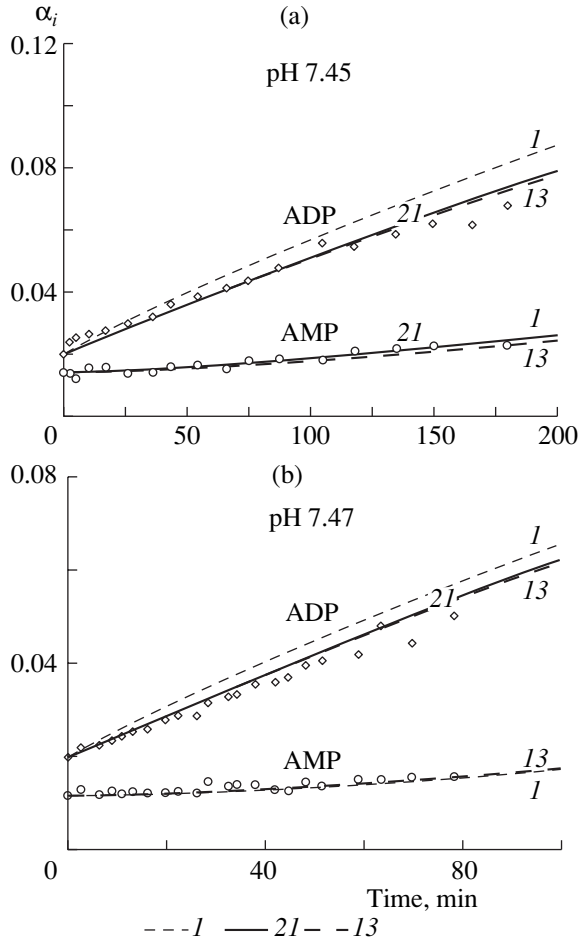

Fig. 2. Kinetic curves of ADP and AMP formation for runs (a) 1 and (b) 12. Points show experimental data. Lines show calculations according to Schemes 2 (1) and 3 (13 and 21). The rate constants for variants 13 and 21 are shown in the text.

where kinetics is determined by the pH-independent hydrolysis pathway. It is seen from the figure that the calculated kinetic curves (*1*) are somewhat higher than the experimental points for the given $[Zn \cdot ATP]_0$ value; an analogous picture was observed in [14] for the run carried out at $[Zn \cdot ATP]_0 = 2.74 \times 10^{-3}$ mol/l and pH = 7.11.

The balance equation at the initial moment of time in the calculations according to Scheme 2 is the same as for pH > 8.5 (Eq. (8) in [9]) and pH 7.1–7.4 (Eq. (7) in [14]) and has the following form: $[ZnATP^{2-}]_0 = (\Sigma[Op])_0 + [Cy]_0 + 2K'_D[Cy]_0^2$, where K'_D is the equilibrium constant of dimer formation from two Cy molecules which is equal to 260 [14]. It is related with K_D, which is the formal equilibrium constant of dimer formation calculated per unit monomer concentration via the formula $K'_D = K_D(3.66)^2$ [14]. Most of the numerical values of rate constants enabling the best description of the concentration dependence of the rates of ADP and AMP formation at pH 7.1 and $[Zn \cdot ATP]_0 = (2.7 \times 10^{-3}–2.74 \times 10^{-1})$ mol/l [14] and the dependence on pH at pH 7.1–8.2 and $[Zn \cdot ATP]_0 = 2.7 \times 10^{-3}$ and 4.2×10^{-3} mol/l in the framework of the dimeric model are described in [9, p. 525]. Other constants are as follows: $k_9 = 1300$ l mol^{-1} min^{-1}; $k_{-9} = 5$ min^{-1}; $k_1 = 7 \times 10^{-3}$ min^{-1}; $k_{20} = 0.49 \times 10^6$ l mol^{-1} min^{-1}; $k_{-20} = 1 \times 10^6$ l mol^{-1} min^{-1}; $k_{23} = 5$ min^{-1}; $k_{-23} = 1300$ l mol^{-1} min^{-1}; $k_{18} = 6 \times 10^{10}$ l mol^{-1} min^{-1}; $k_{-18} = 384$ min^{-1}; $k_{-21} = 6 \times 10^{10}$ l mol^{-1} min^{-1}; $k_{21} = 768$ min^{-1}; and $k_4 = 133$ min^{-1}. The rate constants of steps 3, 4, 10, 11, 7, 6, and 8 are taken from Scheme 1 in [9], and their values are given below when we consider Scheme 3.

The value $K'_D = 260$ l/mol corresponds to $K_D \approx 20$ l/mol [9]. Close values of $K_D = 23$ l/mol and $k_2 = 1.1 \times 10^{-2}$ min^{-1} ($k_2 = 1.2 \times 10^{-2}$ min^{-1} [9]) were obtained earlier in [4] from the initial rates of ATP consumption at pH 7.1. The value of the equilibrium constant of the second stage of P_i deprotonation $[HPO_4^{2-}][H_3O^+]/[H_2PO_4^-] = 6.31 \times 10^{-8}$ mol/l and the fraction of Cy(ZnADP$^-$) in the balance of ZnADP$^-$ species (67 mol %) [12] were used in calculations according to Scheme 2 in [14]. Because ADP in aqueous solution is a mixture of several species, which are in a fast equilibrium, the calculated molar fraction (α_{ADP}) in the general balance of nucleoside-5'-phosphates is the sum

$$\alpha_{ADP} = \alpha(D') + \alpha\{K(ADP)\} + \alpha\{Cy(ADP)\} + \alpha\{Op(ADP)\} + \alpha\{CyOH^-(ADP)\} + \alpha\{OpOH^-(ADP)\} + \alpha\{Op(OH^-)_2(ADP)\} + 2\alpha\{D(ADP)\}.$$

In the calculations according to Scheme 2 in [14], it became evident that the assumption of fast equilibrium between the sum of open species (Σ[Op]), Cy($ZnATP^{2-}$), and dimer D at the initial stage of hydrolysis is a rough approximation. The admissible interval for k_9/k_{-9} appeared to depend noticeably on the initial concentration of Zn · ATP [14]. In the interval of concentrations $[Zn \cdot ATP]_0 = (3.6–27.4) \times 10^{-2}$ mol/l, the admissible interval is 1000/5–1900/5. At an average concentration ($[Zn \cdot ATP]_0 = 7.2 \times 10^{-3}$ mol/l), the corresponding interval is 900/5–1500/5, whereas at $[Zn \cdot ATP]_0 = 2.7 \times 10^{-3}$ mol/l, the admissible interval is 800/5–1300/5. The admissible limits for the rate constants k_9 and k_{-9} at a constant $K'_D = 260$ l/mol are also rather broad: $k_9 = 13$–1300 l mol^{-1} min^{-1} and $k_{-9} = 0.05$–5 min^{-1}. The admissible limits for k_2 are $(1.1–1.3) \times 10^{-2}$ min^{-1}. The admissible limits for $k_{-14}/k_{14} = 2–4$. An analogous situation is also characteristic for runs 3, 5, and 7 (Table 1). Figure 3a shows that, in run 3 (Table 1), the evolution of the kinetic curve for ADP formation is closer to the upper limit for K'_D ($k_9/k_{-9} = 1300/5$) l/mol (curve *1*); the curves corre-

sponding to the lower limit for K'_D (800/5, curve *2*) are far more distant. The lower limit for k_9 (13 l mol^{-1} min^{-1}) and k_{-9} (0.05 min^{-1}) corresponds to curve *3*. It was also found that the dimeric model completely disagrees with the series of experiments at pH 7.1–8.0 and $[Zn \cdot ATP]_0 = 4 \times 10^{-4}$ mol/l (runs 21–25, Table 1). The experimental rates of ADP formation are noticeably lower than those calculated [14]. Figure 3b shows that, even if the value of K'_D corresponds to the lower admissible limit, the calculated kinetic curve of ADP formation is higher than the experimental one. Calculations carried out in [14] showed that, in the range of low Zn · ATP concentrations (4×10^{-4} mol/l), the equilibrium constant of dimer formation from two Cy molecules should be an order of magnitude lower than the corresponding constants at high Zn · ATP concentrations (0.14 mol/l). The rate constants of proton transfer (k_9 and k_{-9}) at low concentrations should also be two orders of magnitude lower than at high concentrations.

A model that takes into account the role of trimeric associates $ZnATP^{2-}$ in the formation of hydrolysis-active species largely eliminated these contradictions (Scheme 3).

Calculations Taking into Account the Role of Trimeric Associates of $ZnATP^{2-}$

The principal difference of the model of Scheme 3 from the model of Scheme 2 in [9] is as follows: in trimeric associates $ZnATP^{2-}$, the rate constant k_{26} of proton transfer from the coordinated water molecule with the formation of a hydrogen bond between γ-phosphate of the first $ZnATP^{2-}$ molecule and atom N1 of the second $ZnATP^{2-}$ molecule (general base catalyst) in Scheme 3 is much higher (by three orders of magnitude) than the corresponding rate constant (k_9) for the dimer. The equilibrium constant for proton transfer in step 26 is more than 30 times as great as the corresponding value for the dimer in step 9 [14].

Calculations carried out in the framework of the trimeric model for pH ≈ 7.1 [14] (Scheme 3) showed that trimeric associates determine the kinetics of ADP and AMP formation at $[Zn \cdot ATP]_0 > 7.2 \times 10^{-3}$ mol/l, and the rate and equilibrium constants for analogous steps are higher for trimers than for dimers. In the range of intermediate concentrations $[Zn \cdot ATP]_0$ ($(2.6–7.2) \times 10^{-3}$ mol/l), the role of trimers is comparable with the role of dimers in creating active centers for the formation of ADP and AMP. Runs 1–20 (Table 1) belong to this interval of Zn · ATP concentrations. At very low initial concentrations of Zn · ATP, trimers virtually do not participate in the formation of active centers of hydrolysis, whereas dimers are formed slowly. At the initial stages of hydrolysis, the kinetics is largely determined by monomeric species. In the calculations according to Scheme 3, we adopted the same ratio $(\Sigma[Op] + [Op'] + [Op'']_0/[Cy]_0 = 2.66$ as in the calculations in the framework of Scheme 2, but the balance

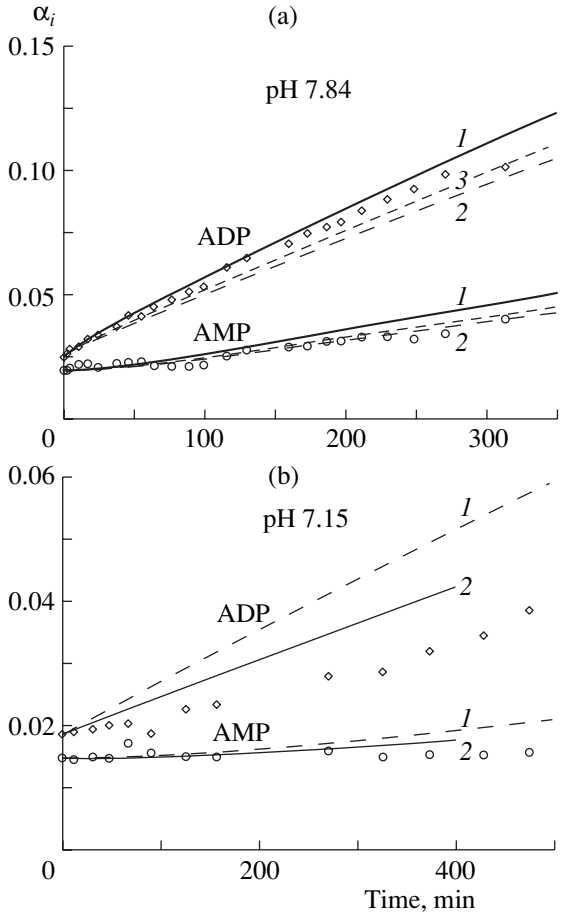

Fig. 3. Kinetic curves of ADP and AMP formation for runs (a) 3 and (b) 21 (Table 1). Lines correspond to calculation according to Scheme 2: (*1*) k_9/k_{-9} = 1200/5 l/mol, (*2*) k_9/k_{-9} = 800/5, (*3*) k_9 = 13 l mol^{-1} min^{-1}, k_{-9} = 0.05 min^{-1}. The points show the experimental kinetic data.

equation for the species that comprise the concentration of $ZnATP^{2-}$ at the initial moment differs from the balance equation used in the calculation of the initial concentrations in Scheme 2.

In Scheme 3, $[ZnATP^{2-}]_0 = [Op]_0 + [Op']_0 + [Op'']_0 + [Cy]_0 + 2[K(ATP)]_0$, and the contributions $[K_{T1}]$ and $[K_{T2}]$ are negligibly small compared to $[K(ATP)]_0$. The balance equation of all species that contribute to the concentration $[NuP]_0$ takes the following form:

$$[NuP]_0 = [CyOH^-]_0 + [OpOH^-]_0 + [Op]_0 + [Op']_0 + [Op'']_0 + [Cy]_0 + 2[K(ATP)]_0 + [ATP^{4-}]_0 + [ADP]_0 + [AMP]_0.$$

Figure 4 shows how the choice of rate constants determining the behavior of trimers in steps 26 and 14' affect the description of kinetic curves in the runs carried out at $[Zn \cdot ATP]_0 = 2.74 \times 10^{-3}$ mol/l at pH 7.5–8.1. For the calculations according to Scheme 3, we used various sets of k_{26} and $k_{14'}$. In variant *8*, k_{26}/k_{-26} = 60 min^{-1}/1 min^{-1}

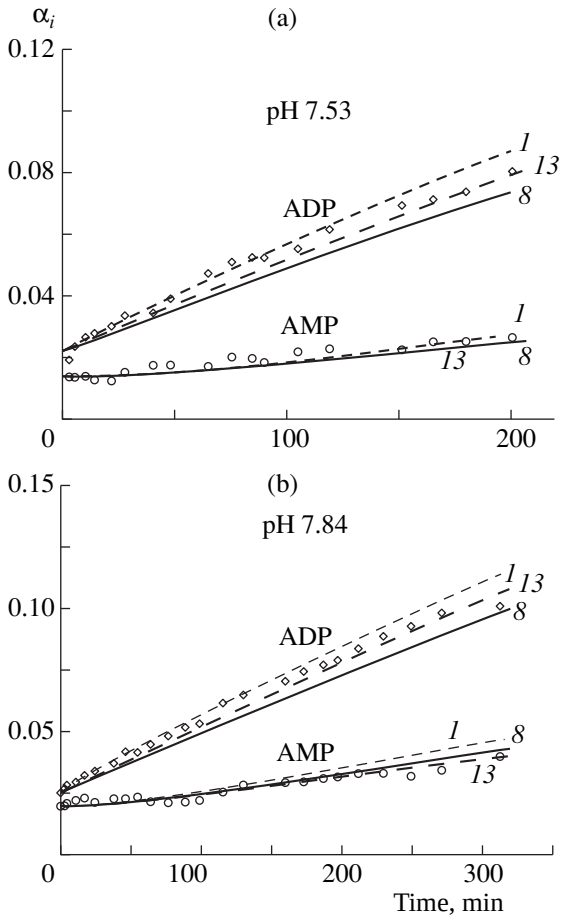

Fig. 4. Kinetic curves of ADP and AMP formation calculated according to Scheme 2 (curves *1*) and Scheme 3 (variants *8* and *13*). Points show experimental data: (a) run 2 and (b) run 3.

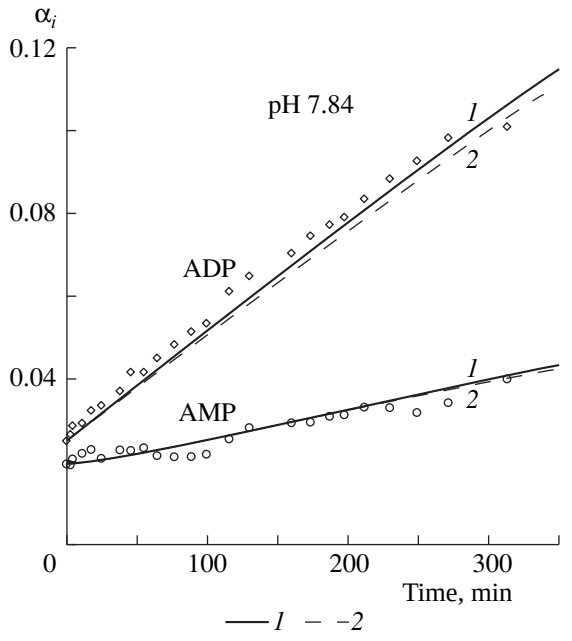

Fig. 5. Kinetic curves of ADP and AMP formation for run 3 (Table 1): (*1*) variant *21*; (*2*) $k_9 = 0.065$ min^{-1} and $k_{-9} = 0.025$ min^{-1}; other constants correspond to variant *21* of Scheme 3. Points show experimental data.

and $k_{-14'}/k_{14'} = 4 \times 10^4$ l mol^{-1} min^{-1}/4×10^3 l mol^{-1} min^{-1} = 10. In variant *13*, $k_{26}/k_{-26} = 750$ min^{-1}/10 min^{-1} and $k_{-14'}/k_{14'} = 4 \times 10^4$ l mol^{-1} min^{-1}/8×10^3 l mol^{-1} min^{-1} = 5.

The rate constants that characterize the transformations of dimers remained constant and equal: $k_{-14} = 1.2 \times 10^4$ l mol^{-1} min^{-1}; $k_{14} = 4 \times 10^3$ l mol^{-1} min^{-1}; $k_2 = 1 \times 10^{-2}$ min^{-1}; $k_{-9} = 0.05$ min^{-1}; $k_9 = 0.13$ min^{-1}; and $k_{15} = 1 \times 10^{-3}$ min^{-1}. The rate constants for trimers in steps 2' and 15' also remained invariable: $k_{2'} = 2.2 \times 10^{-2}$ min^{-1} and $k_{15'} = 2 \times 10^{-3}$ min^{-1}.

Using different variants of calculation according to Scheme 3, we found that an increase in the ratio k_{26}/k_{-26} to 75–90 and a decrease in $k_{-14'}/k_{14'}$ to 5–3 make the description closer to the experimental kinetic curves of ADP formation. The same conclusion for the same variants of constants was drawn earlier for runs carried out at pH 7.1 and $[Zn \cdot ATP]_0 \geq 2.74 \times 10^{-3}$ mol/l [14]. This dependence is partially illustrated by Fig. 4. The transition from the dimeric to trimeric model also makes the description closer to the experimental kinetic curves in the runs shown in Figs. 2 and 4 (curves *1* in Figs. 2 and 4 correspond to the dimeric model).

The values of the main rate constants determining the description of the concentration dependence of the rate of ADP and AMP formation at pH 7.1–7.4, which were finally adopted in calculations reported in [14] and consistent with the runs in this work (variant *21* of the trimeric model) for Scheme 3, are given below. The allowable intervals for significant rate constants are given in parentheses: $k_{-5} = 5.8 \times 10^6$ l mol^{-1} min^{-1}; $k_5 = 2 \times 10^6$ l mol^{-1} min^{-1}; $k_{13} = k_{-13} = 10$ min^{-1}; $k_{-23} = 17$ l mol^{-1} min^{-1}; and $k_{23} = 0.1$ min^{-1};

for the dimer:

$k_9 = 0.13$ min^{-1} (0.065–0.26); $k_{-9} = 0.05$ min^{-1} (0.025–0.1); $k_2 = 9 \times 10^{-3}$ min^{-1} ($(7–11) \times 10^{-3}$); $k_{24} = 1.5 \times 10^{10}$ l mol^{-1} min^{-1}; $k_{-24} = 1.866 \times 10^8$ min^{-1}; $k_{-14} = 1.2 \times 10^4$ l mol^{-1} min^{-1} ($(0.60–1.68) \times 10^4$); $k_{14} = 4 \times 10^3$ l mol^{-1} min^{-1} ($(2.0–5.6) \times 10^3$); $k_{15} = 1 \times 10^{-3}$ min^{-1} ($(1.0–1.7) \times 10^{-3}$); and $k_{-16}[H_2O] = 5$ min^{-1}; $k_{16} = 3 \times 10^4$ l mol^{-1} min^{-1} ($10^4–10^5$). The allowable intervals for k_9/k_{-9} and k_{-14}/k_{14} are (2.0–2.6) and (1.5–3.8), respectively;

for the trimer:

$k_{25} = 1.5 \times 10^9$ l mol^{-1} min^{-1}; $k_{-25} = 2.5 \times 10^8$ min^{-1}; $k_{26} = 900$ min^{-1} (700–1000); $k_{-26} = 10$ min^{-1}; $k_{2'} = 2.2 \times 10^{-2}$ min^{-1} ($(2–2.4) \times 10^{-2}$); $k_{-14'} = 4 \times 10^4$ l mol^{-1} min^{-1} ($(3.6–5.6) \times 10^4$); $k_{14'} = 1.3 \times 10^4$ l mol^{-1} min^{-1} ($(1.17–1.82) \times 10^4$); $k_{-27} = 1.5 \times 10^{10}$ l mol^{-1} min^{-1}; $k_{27} = 2.5 \times 10^9$ min^{-1}; and $k_{15'} = 3 \times 10^{-3}$ min^{-1} ($(2.4–3.6) \times 10^{-3}$). The allowable limits for $k_{-14'}/k_{14'}$ and k_{26}/k_{-26} are

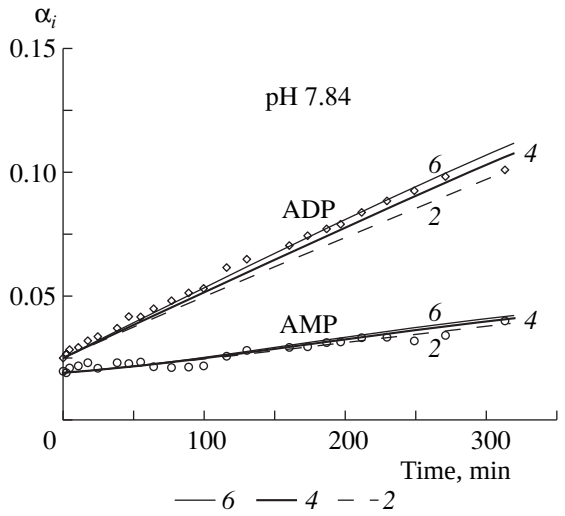

Fig. 6. Kinetic curves of ADP and AMP formation for run 3. Variant *2*: $k_{-5} = 2.9 \times 10^6$, $k_5 = 1 \times 10^6$; variant *4*: $k_{-5} = 5.8 \times 10^6$, $k_5 = 2 \times 10^6$; variant *6*: $k_{-5} = 1.16 \times 10^7$, $k_5 = 4 \times 10^6$ (all constants are in l mol^{-1} min^{-1}). Points show experimental data. Other rate constants remained constant (variant *21* of Scheme 3); $[Zn \cdot ATP]_0 = 2.76 \times 10^{-3}$ mol/l.

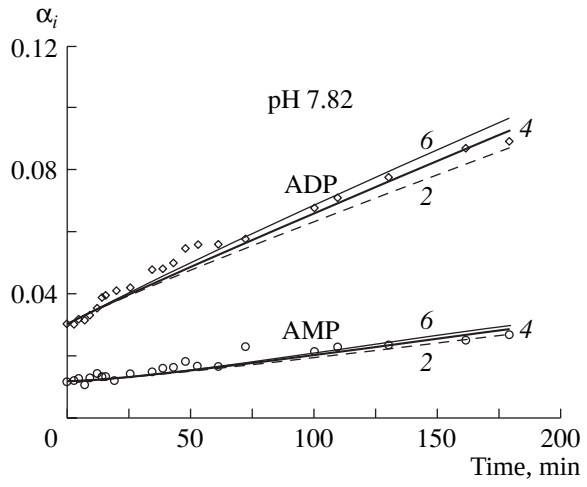

Fig. 7. Kinetic curves of ADP and AMP formation for run 15 carried out at $[Zn \cdot ATP]_0 = 4.23 \times 10^{-3}$ mol/l. Notation of variants is the same as in Fig. 6. Points show experimental data.

(2.8–3.7) and (70–100), respectively. The other constants are the same as in the calculations of Scheme 2.

Figure 5 shows that a decrease in k_9 to 0.065 min^{-1} and k_{-9} to 0.025 min^{-1} (curve *2*) while preserving the equilibrium constant make the agreement of the calculation with experimental data worse. Curve *2* coincides with the curve for calculation where k_9/k_{-9} is lowered to 2.

The rate constants of steps 3, 4, 10, 11, 7, 6, and 8 are taken from Scheme 1 of [9]; $k_4 = 133$ min^{-1} [9]. The values of these rate constants are the same as in the calculation of Scheme 2. We did not specify in [9] the allowable intervals for the rate constants of each of the above steps. We provide them below. In the determination of allowable limits for the rate constant, the equilibrium constant of each step remained constant and equal to the best values. The allowable intervals for the rate constants are given in parentheses: $k_1 = 7 \times 10^{-3}$ min^{-1} ($(6.5–8.0) \times 10^{-3}$); $k_8 = 4.5 \times 10^{-3}$ min^{-1} ($(4.0–5.0) \times 10^{-3}$); $k_7 = 0.23$ min^{-1} (0.207–0.310); $k_{-7} = 7.5 \times 10^{-3}$ min^{-1} ($(6.75–10.0) \times 10^{-3}$); $k_6 = 1.25 \times 10^4$ l mol^{-1} min^{-1} ($(1.0–1.5) \times 10^4$); $k_{-6} = 0.30$ min^{-1} (0.24–0.36); $k_{10} = 1.4 \times 10^4$ l mol^{-1} min^{-1} ($>0.7 \times 10^3$); $k_{-10} = 8 \times 10^4$ l mol^{-1} min^{-1} ($>4 \times 10^3$); $k_{11} = 8 \times 10^4$ l mol^{-1} min^{-1} ($>8 \times 10^3$); and $k_{-11} = 1.4 \times 10^4$ l mol^{-1} min^{-1} ($>1.4 \times 10^3$). The allowable intervals for the ratios k_7/k_{-7} and k_6/k_{-6} are (27–37) and $(3.8–4.2) \times 10^4$ l/mol, respectively. The allowable intervals for the ratios k_{-10}/k_{10} and k_{11}/k_{-11} are the same and equal to (4.3–7.1).

Fitting the values of k_5 and k_{-5} was carried out in [9] at pH 8.7–9.0, which is the most sensitive to these constants (the rate laws of steps 5 and –5: $w_5 = k_5[Cy][H_3O^+]$; $w_{-5} = k_{-5}[Op''][H_3O^+]$ involve $[H_3O^+]$). The best variant for the description of kinetic curves is variant *4* ($k_{-5} = 5.8 \times 10^6$ l mol^{-1} min^{-1}; $k_5 = 2 \times 10^6$ l mol^{-1} min^{-1}). The interval of allowable values for k_{-5} is $(8.7–2.9) \times 10^6$ l mol^{-1} min^{-1} and for k_5, $(1.0–3.0) \times 10^6$ l mol^{-1} min^{-1}. Figure 6 illustrates the effect of choosing the rate constant of step 5 on the kinetic curves at $[Zn \cdot ATP]_0 = 2.76 \times 10^{-3}$ mol/l. For the higher concentration $[Zn \cdot ATP]_0 = 4.23 \times 10^{-3}$ mol/l, we observed an analogous dependence (Fig. 7), and the sensitivity to the values of constants for step 5 at the same pH (Figs. 6 and 7) is somewhat higher at a higher concentration of Zn · ATP. At pH 7.5–8.2, as at pH > 8.5, the best variant for the description is variant *4*, and the sensitivity of description to the values of k_{-5} and k_5 increases with an increase in pH. At very low concentrations $[Zn \cdot ATP]_0 = 4 \times 10^{-4}$ mol/l (at pH 7.66), there is no sensitivity at all to the values k_{-5} and k_5, and a small difference only reveals itself at higher pH (pH 8.19) (Fig. 8). It is seen from Figs. 6–8 that in the analyzed range of pH, the constants and the rate expression of step 5 is the same as at pH 8.7–9.0. Thus, the participation of $[H_3O^+]$ in the isomeric conversion Op $\rightleftharpoons$ Cy, which was earlier proposed to explain the apparent decrease in the rate of the process Op $\rightleftharpoons$ Cy at pH > 8.5, turns from a hypothesis into an experimentally proven fact. The mechanism of the isomeric conversion Op $\rightleftharpoons$ Cy that we propose is based on the kinetic description of step 5 and naturally follows from the structures of Op and Cy conformers proposed earlier, taking into account different hydrations of the terminal phosphate in these species (see Fig. 1 in [9]). We supposed that isomeric conversion occurs in three steps (Scheme 2a in [9]). Note that the step for the formation of the pentacovalent intermediate Op' (12) and pseudorotation step (13) are fast, and the slow step in iso-

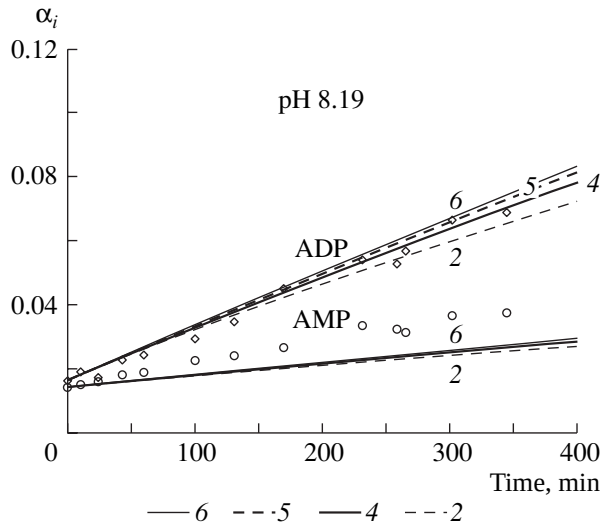

Fig. 8. Kinetic curves of ADP and AMP formation for run 25 carried out at $[Zn \cdot ATP]_0 = 0.400 \times 10^{-3}$ mol/l. In variant *5*: $k_{-5} = 8.7 \times 10^6$, $k_5 = 3 \times 10^6$ l mol^{-1} min^{-1}; the notation of other variants is the same as in Figs. 6 and 7. Points show experimental data.

meric transformation is step 5. In step 5, the abstraction of OH from the apical position takes place with the participation of H_3O^+, the formation of the coordinated H_2O molecule, and the hydration of terminal phosphate in the $ZnATP^{2-}$ Cy-species. Note also that the pivot for pseudorotation [17] is the bridging P_γ–OP_β bond. In pseudorotation, OH that earlier belonged to the terminal phosphate appears in the apical position with respect to the P_γ atom of Op". In the sequence of steps of isomeric transformation, steps are present in which OH^- of γ-phosphate substitutes for OH^- of the medium. In the scheme of ion transformation $CyOH^- \rightleftharpoons OpOH^-$, these steps are fast [9], and the slow step is pseudorotation (7). In the scheme of Op $\rightleftharpoons$ Cy transformation, the exchange of OH of γ-phosphate with H_2O in step 5 determines the rate of conformational transformation. ^{18}[O] exchange between oxygen atoms of P_i and H_2O in the intermediate steps of ATP hydrolysis and synthesis is characteristic of ATP-ases [18–23] and, as we believe, is related to the mechanism for the formation and transformation of $MATP^{2-}$ species that are active in hydrolysis: Cy and $CyOH^-$.

Scheme 1 shows the proposed mechanism for the formation of ADP in the pH-independent channel of dimeric associate $ZnATP^{2-}$ hydrolysis. In slow step 2 of dimer hydrolysis, the proton that participates in the formation of the hydrogen bond $N_1\cdots H^+\cdots O^-$–P_γ transfers to the hydrogen bond $N_1\cdots H^+\cdots O^-$–P_β of the $ZnADP^-$ formed. In the intermediate complex $D'\{Cy(ZnADP^-) \cdot Cy(ZnATP^{2-})H^+(HPO_4^{2-})\}$, the bridging bond between P_γ and –OP_β is cleaved. In the subsequent fast reversible step 16, HPO_4^{2-} "withdraws" H^+ from the hydrogen bond and cleaves it, while the ligand $H_2PO_4^-$ at Zn^{2+} is replaced by H_2O. The K(ADP) complex is formed in which $Cy(ZnATP^{2-})$ and $Cy(ZnADP^-)$ are only bound via stacking interaction. The phosphate chain of $ZnADP^-$ is hydrated, and $H_2PO_4^-$ transfers to the aqueous medium. The K(ADP) complex is in equilibrium with the monomeric species of $Cy(ZnADP^-)$ and $Cy(ZnATP^{2-})$ (step 17). The reversible formation of ADP is the consequence of the intermediate formation of a hydrogen bond. Only step 2, which characterizes the proton transfer in the dimer with the formation of D' [14], and step 16 are reversible. The reversibility is noticeable at $[ZnATP^{2-}]_0 \geq 0.078$ mol/l at pH ≈ 7.1. Under the experimental conditions specified in Table 1, ADP is formed virtually irreversibly (the fraction of species D' is two to three orders of magnitude smaller than the fraction of D). Scheme 1 assumes that a decrease in the nucleophilicity of the leaving group largely determines the energetics of the P_γ–OP_β bond cleavage (step 2). At the formation of D', both H^+ of the hydrogen bond and Zn^{2+} are bound to the β-phosphate group. When the monomeric $CyOH^-$ reacts, only Zn^{2+} that forms a bond with the β-phosphate group decreases the nucleophilicity of the leaving group. However, the cleavage of the P_γ–OP_β bond does not itself mean the liberation of products to the medium. We assume that the product in both cases (in the associate and in the monomer) is formed like $Cy(ZnADP^-)$. The estimate of pK_{aCy} for $ZnADP^-$ made in [14] shows that $K_{aCy} \approx 6.4 \times 10^9$ mol/l for $ZnADP^-$, whereas $K_{aCy} \approx 0.84 \times 10^9$ mol/l for $ZnATP^{2-}$ [9]. This means that the terminal phosphate in the $ZnADP^-$(Cy) complex is hydrated much more strongly than in the $ZnATP^{2-}$(Cy) complex, the hydrogen bond of water is stronger in $ZnADP \cdot OH_2$(Cy), and $ZnADP^-$ is much more ionized at the pH under consideration than $ZnATP^{2-}$. Therefore, although the equilibrium of step 16 is shifted toward D' (the ratio $k_{16}/k_{-16}[H_2O] \approx 6000$ l/mol in the trimeric model [14]), the abstraction of $H_2PO_4^-$ occurs: D' is too strained a structure, and cannot hold the bulky $H_2PO_4^-$ ligand. It is likely that the hydration of the terminal phosphate in $ZnADP^-$ contribute to the general change in the free energy in hydrolysis. In connection with this, we note that, according to [12, 13], the fraction of Cy in the balance of $ZnADP^-$ species in the aqueous solution (67 mol %) is much larger than the fraction of Cy in the balance of $ZnATP^{2-}$ (28%). A higher acidity of coordinated water in the ADP^{3-} complexes compared to the acidity of ATP^{4-} complexes is also known for Al^{3+} [24].

Figure 9 shows changes in the calculated concentrations (molar fractions) of the main intermediate products and final products (ADP and AMP) in hydrolysis

carried out at the very low concentration $[Zn \cdot ATP]_0 = 0.400 \times 10^{-3}$ mol/l. The molar fractions of different species are given in fractions relative to the initial concentration of nucleoside-5'-phosphates (NuP) in all figures. The experimental kinetic curves for the formation of ADP and AMP are also compared with the calculated ones. Trimers virtually do not affect the description of kinetics for this series of experiments; $\Sigma([T1] + [T2])$ is equal to 10^{-4}–10^{-5}, the fraction of $(DOH^-)H^+ \cdot Op$ and $(DOH^-)H^+ \cdot Cy$ being somewhat higher. The concentration of $Op(OH^-)_2$ reaches the maximum value at an early stage of hydrolysis and further changes only slightly. The concentration of dimer D passes through a flat maximum, and the fraction of dimer in the balance of $[NuP]_0$ species decreases with an increase in pH. The fraction of dimeric $(DOH^-)H^+$ species formed in step 14 increases as the dimer is accumulated. Table 2 shows the contribution of different forms to the relative specific rate of ADP formation (r_{ADP})[1] at the moment of attaining the maximum dimer concentration. Because the maximum of the dimer concentration is very flat, the calculation refers to the middle of the flat maximum (≈250 min for all runs of series III). Table 2 also specifies the contributions of transformations of various species to the relative specific rate of AMP formation (r_{AMP}) for two moments of time: the time of reaching the maximal concentration of $Op(OH^-)_2$ and the time when the induction period of AMP formation ends. The results of the calculation show that the relative contribution of D to the rate of ADP formation decreases with an increase in pH, and the relative contribution of monomeric $CyOH^-$ increases. At pH 8.19, this contribution determines the kinetics of ADP accumulation. With an increase in pH, the relative contributions of the dimeric associates to the kinetics of AMP accumulation decrease when induction ends, and the contribution of monomeric $Op(OH^-)_2$ species increases. At pH > 8, this contribution determines the kinetics of AMP accumulation both at the initial stage and after induction.

Figures 10–12 for runs carried out at higher concentrations $[Zn \cdot ATP]_0 = (2.74 \pm 0.05) \times 10^{-3}$ mol/l show changes in the calculated concentrations of intermediate products [ADP] and [AMP] in the course of hydrolysis (variant *21* of the trimeric model). At the initial portions of kinetic curves, trimers T1 and T2 are formed very rapidly (the calculated maximum of their formation is 0.2–0.5 min). In this case, the initial rate of ADP formation is determined by $\Sigma([T1] + [T2])$ to an extent of 82% and by $[CyOH^-]$ to an extent of 14.7% at pH 7.45; 69 and 29%, respectively, at pH 7.84; 50 and 48.3% at pH 8.14; and 43 and 56% at pH 8.24. The contributions of the dimer to the initial rate are small (0.5–3%). When the maximal dimer concentration is achieved, the contributions of the dimers and trimers are close (Table 3). The contribution of the monomeric species $CyOH^-$ to ADP formation increases with an increase in pH. At pH 8.24, the contribution of $[CyOH^-]$ is approximately equal to the sum of associate contributions. The contribution of trimers to the formation of AMP dominates both at the initial stage and after the

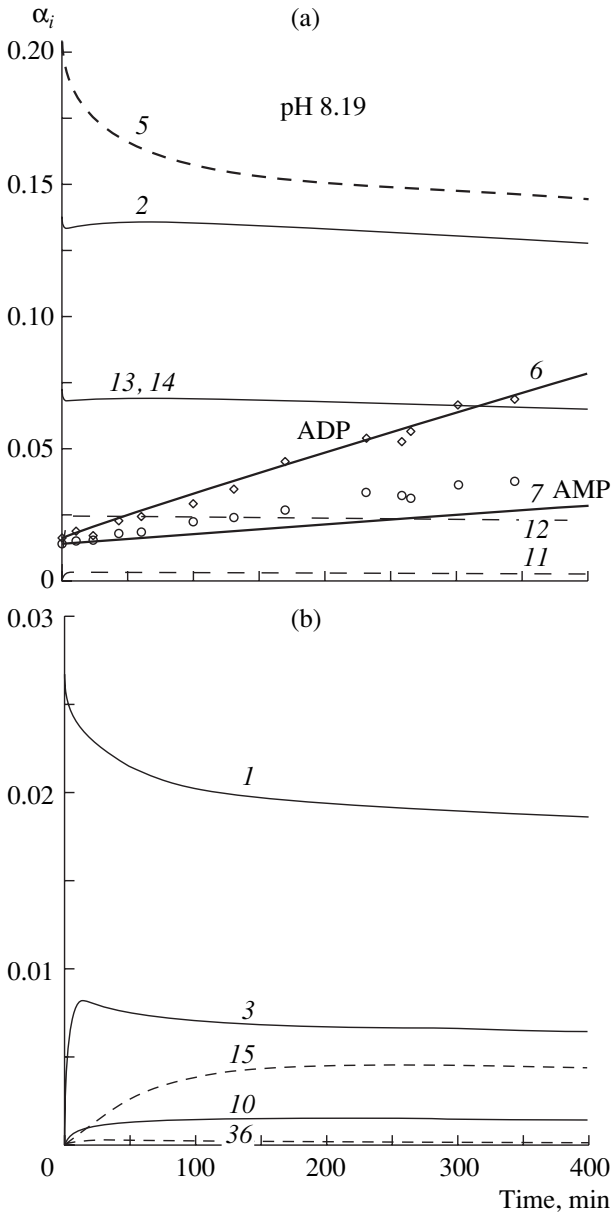

Fig. 9. Changes in the relative concentrations of intermediate products in the course of hydrolysis carried out at pH 8.19 and 50°C (run 25). $[Zn \cdot ATP]_0 = 0.400 \times 10^{-3}$ mol/l. Curves: (*1*) $CyOH^-$, (*2*) $OpOH^-$, (*3*) $Op(OH^-)_2$, (*5*) Cy, (*6*) ADP, (*7*) AMP, (*10*) D, (*11*) $Cy'OH^-$, (*12*) $Op'OH^-$, (*13*) Op', (*14*) Op", (*15*) $(DOH^-)H^+$, and (*36*) $(DOH^-)H^+ \cdot Op$. Points show experimental data. Calculation was carried out according to Scheme 3 assuming the trimeric model (variant *21*).

[1] $r_{ADP} = [D] \times 0.9 + ([T1] + [T2]) \times 2.2 + [CyOH^-] \times 0.7$; the coefficients reflect the ratio of the rate constants in steps 2, 2', and 1. $r_{AMP} = [(DOH^-)H^+] \times 1 + \{[(DOH^-)H^+ \cdot Cy] + [(DOH^-)H^+ \cdot Op]\} \times 3 + [Op(OH^-)_2] \times 4.5$; the coefficients reflect the ratio of the rate constants in steps 15, 15', and 8.

Table 2. Contributions from different species to the relative specific rate of ADP and AMP formation at the concentrations $[Zn \cdot ATP]_0 = (0.401 \pm 0.001) \times 10^{-3}$ mol/l. Calculation according to Scheme 3

Run	pH	Time of attaining $[D]^*_{max}$, min	Contributions to r_{ADP}, %			Time of attaining		Contributions to r_{AMP}, %					
			$CyOH^-$	D	Σ(T1 + T2)	$[Op(OH^-)_2]_{max}$, min	$\tau_{ind, AMP}$, min	$Op(OH^-)_2$		$(DOH^-)H^+$		$\Sigma(DOH^-)H^+ \cdot M$	
						1	2	1	2	1	2	1	2
21	7.15	250	33.4	56.4	10.2	24		29.7		29.1		41.2	
							192		6.2		65.3		28.5
**	7.44	250	51.1	41.4	7.5	20		53.6		18.1		28.3	
							175		13.5		68.9		17.6
21	7.66	250	63.9	30.7	5.4	18		70.5		11.5		18.0	
							150		32.7		50.8		16.5
23	7.81	250	72.5	23.5	3.9	16		81.2		7.1		11.7	
							90		54.1		32.7		13.2
24	8.00	250	81.7	15.8	2.5	16		89.3		4.3		6.4	
							54		77.9		14.8		7.3
25	8.19	250	89.3	9.4	1.3	14		95.3		1.9		2.8	
							26		93.0		3.9		3.1

Notes: * $[D]_{max}$ and $[Op(OH^-)_2]_{max}$ are the maximal concentrations of D and $Op(OH^-)_2$.
** [14].
1—Contribution to the relative specific rate of AMP formation (r_{AMP}) at the moment the maximal concentration of $[Op(OH^-)_2]$ is achieved.
2—Contribution to the relative specific rate of AMP formation (r_{AMP}) at the end of the induction period.

Table 3. Contributions of various species to the relative specific rate of ADP and AMP formation at $[Zn \cdot ATP]_0 = (2.74 \pm 0.05) \times 10^{-3}$ mol/l. Calculation according to Scheme 3

Run	pH	Time of attaining $[D]^*_{max}$, min	Contributions to r_{ADP}, %			Time of attaining		Contributions to r_{AMP}, %					
			$CyOH^-$	D	Σ(T1 + T2)	$[Op(OH^-)_2]_{max}$, min	$\tau_{ind, AMP}$, min	$Op(OH^-)_2$		$(DOH^-)H^+$		$\Sigma(DOH^-)H^+ \cdot M$	
						1	2	1	2	1	2	1	2
1	7.45	63	9.8	40.8	49.4	15		5.4		7.2		87.4	
							57		2.2		18		79.8
2	7.53	79	11.9	40.3	47.8	14		7		6.8		86.2	
							53		3		17.6		79.4
3	7.84	202	24.3	38.9	36.7	13		17.5		6.3		76.2	
							45		10.6		17.8		71.6
5	8.05	244	36.6	33.7	29.6	11		32.9		4.9		62.1	
							37		24.2		15.3		60.5
7	8.14	242	43.7	30.3	26	11		41.7		4.6		53.7	
							32		34.4		13.2		52.4
8	8.21	200	49.3	27.2	23.5	11		49		4.3		46.7	
							27		43.3		10.5		46.2
9	8.24	220	52.1	26.1	21.8	11		52.5		4		43.5	
							27		47.1		10.1		42.8
11	8.50	100	73.4	14.9	11.6	10	10	80.4		2		17.6	

Note: See notes 1 and 2 for Table 2.

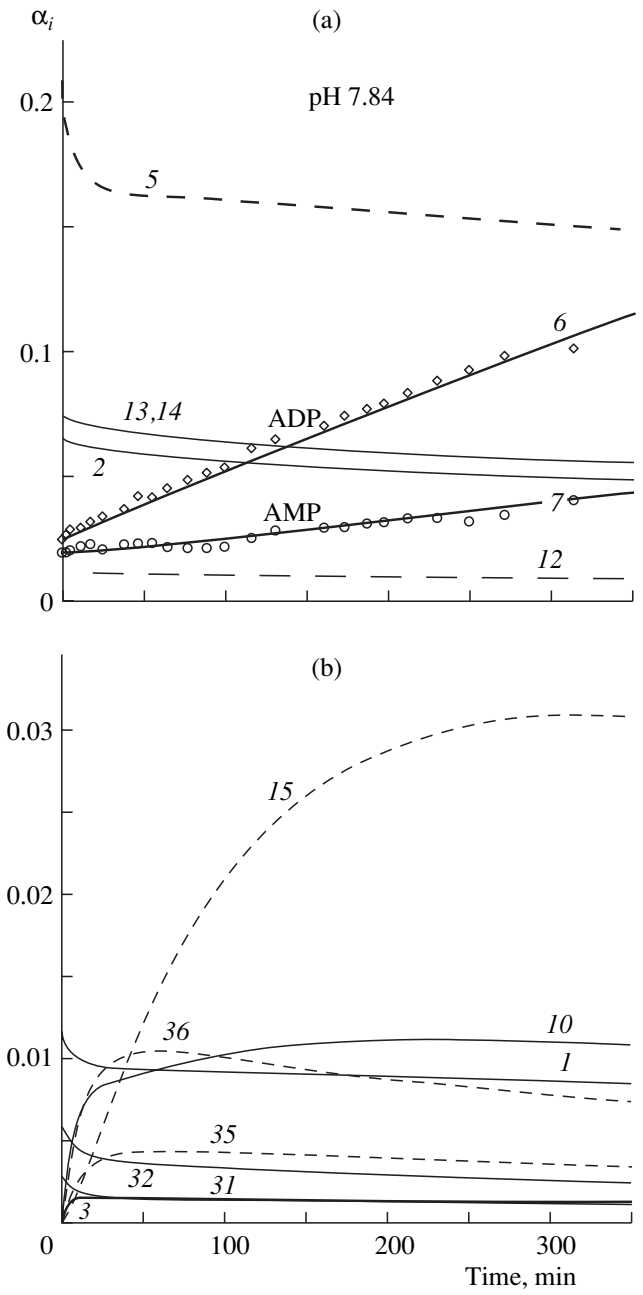

Fig. 10. Kinetic curves of ADP and AMP formation and changes in the concentrations of intermediates in run 3 [Zn · ATP]$_0 = 2.76 \times 10^{-3}$ mol/l. Notation for intermediates is the same as in Fig. 9. Points show experimental data; *31*—T1; *32*—T2. *35*—$(DOH^-)H^+$ · Cy.

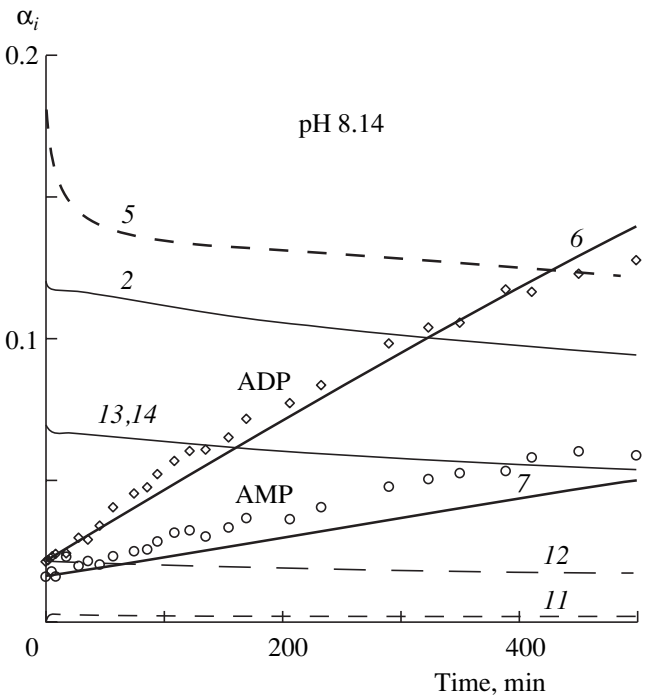

Fig. 11. Kinetic curves of ADP and AMP formation and changes in the concentrations of intermediates in run 7. Notation for intermediates is the same as in Figs. 9 and 10. Points show experimental data.

end of the induction period at pH < 8.1. At pH 8.1–8.2, the contributions of trimers and monomers are close. Only at pH 8.50 does the monomeric species $Op(OH^-)_2$ have a dominant contribution (80.4%) after the end of the induction period of AMP formation.

When pH changes from 7.47 to 7.82 in the runs of series II, the relative contribution of D to the balance of the species diminishes. The relative contribution of $(DOH^-)H^+$ grows. The fractions of $CyOH^-$ and $Op(OH^-)_2$ grow, and the fraction of Cy decreases. Comparison of data in series I and II at close pH (runs 2, 12; 3 (Fig. 10) and 15) shows that, at higher concentrations, the relative fractions of [D] and Σ([T1] + [T2]), as well as the relative fraction of $[(DOH^-)H^+ \cdot M]$ (where M = Cy or Op), increase. The initial rate of ADP formation in the runs of series II is determined by Σ([T1] + [T2]) to an extent of 91% and by $[CyOH^-]$ to an extent of 7% at pH 7.47; 82.4 and 16% at pH 7.82; and 64 and 35% at pH 8.20. The contributions of the dimer to the initial rate are insignificant (<2%). When the maximal dimer concentration is achieved, the contributions of trimers are greater than the contributions of dimers (Table 4). The contribution of the monomeric species to the formation of ADP in the considered range of pH is smaller than the sum of the contributions of associates. Trimers have the dominant contribution to r_{AMP} both at an early stage and after the induction period at pH 7.47–8.20, and the relative contribution of trimers in the runs of series II is much greater than in the runs of series I.

The values of rate constants found from calculation using Scheme 3, as well as changes in the calculated concentrations of intermediate products in the course of hydrolysis, allow one to find the quantitative estimates of the ratio of the rates of the isomeric conversion Op $\rightleftharpoons$ Cy, which is responsible for making up Cy and the rates of hydrolysis product (ADP and AMP) formation from intermediate products. The latter characterize bond cleavage in the phosphate chain. Table 5 shows the

Table 4. Contributions from different species to the relative specific rate of ADP and AMP formation at $[Zn \cdot ATP]_0 = (4.20 \pm 0.07) \times 10^{-3}$ mol/l. Calculation according to Scheme 3

Run	pH	Time of attaining $[D]^*_{max}$, min	Contributions to r_{ADP}, %			Time of attaining		Contributions to r_{AMP}, %					
			$CyOH^-$	D	$\Sigma(T1 + T2)$	$[Op(OH^-)_2]_{max}$, min	$\tau_{ind, AMP}$, min	$Op(OH^-)_2$		$(DOH^-)H^+$		$\Sigma(DOH^-)H^+ \cdot M$	
						1	2	1	2	1	2	1	2
12	7.47	57	6.5	34.6	58.9	14		3.1		5.1		91.8	
							42		1.5		11.4		87.1
14	7.62	60	9.6	32.9	57.5	12		5.4		4.5		90.1	
							37		2.8		11.1		86.2
15	7.82	169	16.1	35.8	48.1	11		10.1		4.3		85.6	
							31		6.3		10.6		83.1
17	8.00	≈80	24.3	27.8	47.8	10		18.4		3.9		77.6	
							27		13.4		10.1		76.5
20	8.20	≈80	36.4	23.9	39.7	10		32.3		3.6		64.1	
							21		28.5		7.8		63.7

Note: See notes 1 and 2 for Table 2.

Table 5. The rate for the formation of the main Cy species that is active in hydrolysis in step 5 calculated according to the trimeric model (Scheme 3) and the overall rates of hydrolysis product formation (ADP and AMP) from intermediate products

pH	Series I						Series II						Series III			
	7.53		7.84		8.14		7.47		7.82		8.20		7.44		8.19	
$[NuP]_0 \times 10^3$, mol/l	2.90		2.89		2.87		4.48		4.47		4.44		0.421		0.419	
Time, min	14	150	13	202	11	242	14	57	11	169	10	80	20	250	14	250
$(w_{Op'' \to Cy} - w_{Cy \to Op''}) \times 10^7$, mol l^{-1} min^{-1}	43	12	28.7	13.8	16	17	97.4	48	61.6	24.8	28.9	28.9	1.3	0.43	0.84	2.47
$(w_{CyOH^- \to ADP} + w_{D \to ADP} + w_{\Sigma T \to ADP} + w_{Op(OH^-)_2 \to AMP} + w_{(DOH^-)H^+ \to AMP} + w_{\Sigma(DOH^-)H^+ \cdot M \to AMP}) \times 10^7$, mol l^{-1} min^{-1}	9.5	10.3	8.9	9.6	9.3	8.9	21.9	23.1	19.0	19.3	18.6	17.0	0.27	0.34	0.90	0.78

value ($w_{Op'' \to Cy} - w_{Cy \to Op''}$), which is the rate for the formation of the main product Cy($ZnATP^{2-}$) in step 5. This product forms the dimer, trimers, and $CyOH^-$ (via fast ionization).

$$w_{CyOH^- \to ADP} + w_{D \to ADP} + w_{\Sigma T \to ADP} + w_{Op(OH^-)_2 \to AMP} + w_{(DOH^-)H^+ \to AMP} + w_{\Sigma(DOH^-)H^+ \cdot M \to AMP}$$

is the sum of the rates for the formation of final products (ADP and AMP) by the bond cleavage in the phosphate chain. The calculations refer to the two moments of time: the time when the maximal concentration of $Op(OH^-)_2$ is achieved at the initial portion of the kinetic curve and the time when the maximal dimer concentration is achieved (this one is close to the end of the observed kinetic curve). Calculations were carried out for the runs of series I at different pH, series II, and series III. At the initial stage of hydrolysis in series I and II when the rate of ADP formation is largely determined by the associates and decreases, the sum of the rates of final product formation is lower than the rate of Cy formation in step 5. The higher the pH, the smaller this difference. In the course of hydrolysis, the rate of Cy formation in step 5 approaches the sum of the rates of phosphorus anhydride bond cleavage. At very low concentrations and pH 8.19, even for the initial portion, the overall rate of P–O–P bond cleavage is close to the rate of Cy formation, whereas the cleavage of P–O–P bonds is slow in the course of hydrolysis. At pH ≥ 8.5, the overall rates of final product formation are noticeably higher than the rates of filling Cy up in step 5 at the initial stage of hydrolysis, and the isomeric transformation controls the formation of final products (see Table 6 in [9]).

The proposed model allows one to adequately describe the complete set of experimental data analyzed in [9, 14] and in this work over all the ranges of pH and concentrations studied. The model that accounts for trimeric associates is more correct than the dimeric one, because it does not assume equilibrium between active monomeric and dimeric species at the initial stage. The reason for the increase in the number of active centers of hydrolysis in trimers (T1 and T2) compared to dimer D is the spatial position of the third molecule whose coordinated water stabilizes coordinated OH^- of the first $ZnATP^{2-}$ molecule by a hydrogen bond. Coordinated OH^- is formed by proton transfer during the formation of a hydrogen bond in the reaction center of the hydrolysis. Figure 13 shows the proposed structure of the trimeric $ZnATP^{2-}$ associate T2 (D · Op). The spatial structure of the trimer was considered in detail in [14]. The trimeric associate includes two monomeric cyclic molecules Cy($ZnATP^{2-}$) in conformations **A** and **B** and the open species $ZnATP^{2-}$ (in Op-conformation **B**), positioned below the second Cy molecule. The P_γ–OP_β bond cleaves in the first

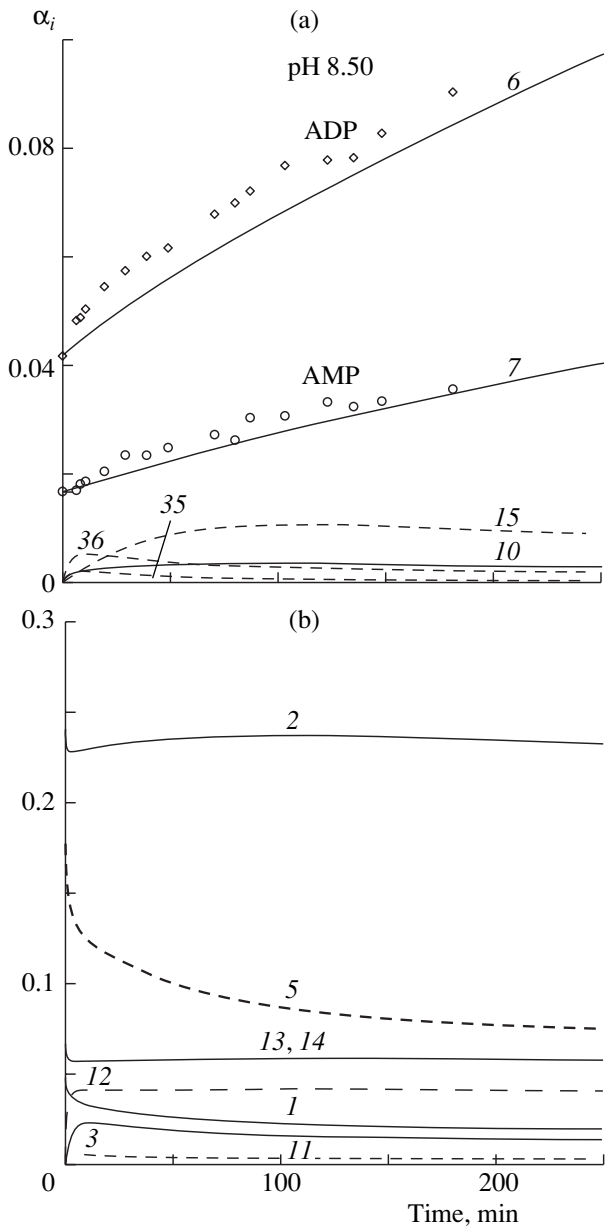

Fig. 12. Changes in the concentrations of intermediates in the course of hydrolysis carried out at $[Zn \cdot ATP]_0 = 2.70 \times 10^{-3}$ mol/l (run 11). Points show experimental data.

Cy($ZnATP^{2-}$) molecule (**B** conformer). This is a substrate in which the reaction center of the hydrolysis is formed by H^+ transfer from water coordinated to γ-phosphate, and a hydrogen bond is formed between the γ-phosphate of the first molecule and atom N1 of the second Cy molecule (conformation **A**). The second molecule (a donor of N1 and a general base catalyst for the hydrolysis of the first molecule) is situated beneath the first Cy molecule. The third molecule $Op(ZnATP^{2-} \cdot OH_2)$ (conformation **B**) is a cocatalyst of the hydrolysis. Its coordinated water (acid) solvates the coordinated OH^- ion of the first molecule and forms a hydrogen bond with it,

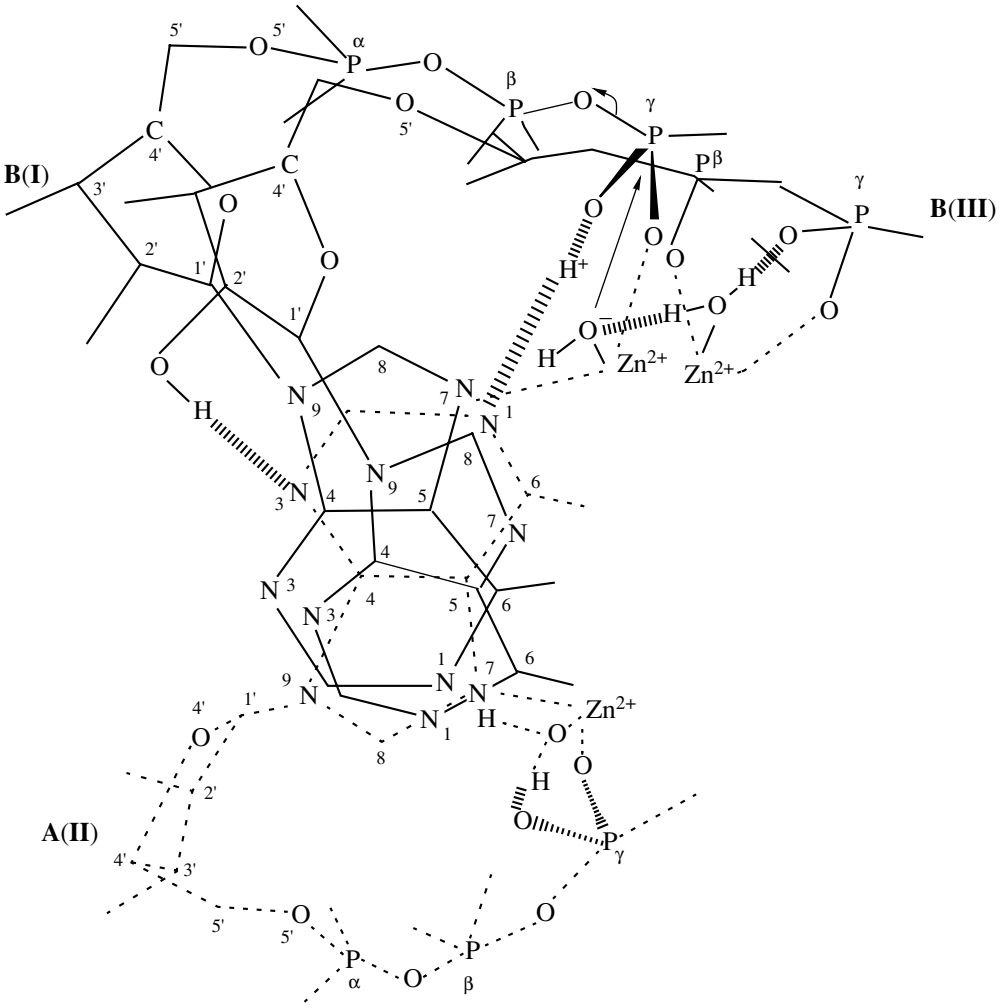

Fig. 13. Assumed structure of the trimeric associate T2 (D · Op): The first **B** (**I**) is the Cy substrate that forms the reaction center of the hydrolysis; **A** (**II**) is the Cy catalyst and N1 donor for the hydrogen bond with O^{-}–P_{γ} of the first molecule; **B** (**III**) is the third $ZnATP^{2-} \cdot OH_2$(Op), a cocatalyst.

thus accelerating the formation of the $Zn^{2+}OH^{-}$ ion. The latter is a nucleophile that attacks γ-P of the first $ZnATP^{2-}$ molecule. The bases of all the three $ZnATP^{2-}$ molecules are bound via stacking-interaction. The third molecule initially binds with the K(ATP) complex via stacking-interaction. In this complex, the first and second Cy($ZnATP^{2-}$) molecules were only bound via stacking-interaction (step 25 of Scheme 3). Thus, the adenine base of the third molecule attaches to the place that is distant from the reaction center of the hydrolysis. An increase in the rate of formation of the active center of the hydrolysis of the first molecule occurs due to interaction between the phosphate chains of the first and third $ZnATP^{2-} \cdot OH_2$ molecules, which results in the formation of the hydrogen bond between coordinated H_2O and the coordinated OH^{-} ion. The general base catalysis by coordinated water of the third molecule is responsible for an increase in the rate constant of proton transfer in trimers (k_{26}) compared to the rate constant for the dimer (k_9), an increase in the equilibrium constant of proton transfer $k_{26}/k_{-26} = 90$ in trimers compared to that for the dimer ($k_9/k_{-9} = 2.6$), and an increase in the rate constant of OH^{-} substitution in trimers ($k_{-14'} = 4 \times 10^4$ l mol^{-1} min^{-1}) compared to that for the dimer ($k_{-14} = 1.2 \times 10^4$ l mol^{-1} min^{-1}).

A similar effect takes place in enzymatic catalysis. The H^{+}–AT-ase complex (F_1F_0) catalyzes the synthesis of ATP in oxidative phosphorylation. The catalytic part F_1 is formed of several subunits and acts as ATP-ase. The mechanism of ATP hydrolysis by the mitochondrial F_1 factor and the F_1 factor from *E. coli* has been studied: in the first catalytic site ATP is hydrolyzed only slowly ("uni-site" hydrolysis), but when the ATP binds to the second and third sites, ATP is hydrolyzed at the first site with the release of products at a maximal rate ("multisite" hydrolysis) due to the positive cooperativity between the three catalytic sites [21, 22, 25, 26]. In the case of two (or three) sites of

hydrolysis, the rate of ATP hydrolysis increases 10^6 times in the case of mitochondrial F_1 and 10^4–10^5 times for *E. coli* F_1. There is no doubt that the structure of F_1 ATP-ase is much more complex than the structure of trimer T_2, and different catalytic centers of the ATP-ase probably belong to different subunits of the catalytic complex. Nevertheless, we may assume that the accelerating effects in trimers and the positive cooperativity between the catalytic sites have a common nature: general acid catalysis by the coordinated H_2O molecule, belonging to ATP in one of the sites, of the process of active nucleophile formation in another catalytic site, and the interaction of sites via hydrogen bonds. In enzymes, this interaction occurs via changes in the conformations of catalytic subunits. It is likely that the coordinated H_2O molecules belonging to a protein participate in proton transfer through the system of hydrogen bonds.

Kinetic Scheme 3 can be made more complex by considering some fine effects that were neglected before. It is seen from Figs. 11 and 12a that, at the initial portion of the kinetic curve of ADP formation ($\approx$ <150 min), the calculated kinetic curves of ADP formation (6) deviate from the experimental ones. Although these deviations are small, they are well reproducible: in runs 8 and 9, there are similar deviations at the initial portion. Moreover, the deviations steadily increase with an increase in pH. They reveal themselves in the narrow range of pH 8.1–8.5. At pH 8.24 they are noticeable. At pH 8.50, they are at maximum. Analogous deviations in the same range of pH were also observed in the runs of series II. Our calculations showed that the initial portion of the kinetic curve at which deviations are observed is insensitive to the choice of the rate constants and the equilibrium constant of step 26. It is also poorly sensitive to the equilibrium constant of step 14'. The differences in the kinetic curves of ADP formation associated with changes in the rate constants of step 5, the equilibrium constant of step 14', and the rate constants of steps 2 and 2' reveal themselves after 170–200 min in this range of pH. Deviations of the initial portion in the range where the concentration of OH^- noticeably increased show that we overestimate the rate of decrease in the concentrations of D, T1, and T2 in steps 14' and 14 in this range of pH by using the rate laws $w_{-14'} = k_{-14'}[T2][OH^-]$, $w_{-14'} = k_{-14'}[T1][OH^-]$, and $w_{-14} = k_{-14}[D][OH^-]$, in which the rates are proportional to $[OH^-]$ at the moments of time when $(DOH^-)H^+$ and $\Sigma(DOH^-)H^+ \cdot M$ are accumulated in the induction period. Deviations are observed in the narrow range of pH 8.1–8.5, where the contributions of associates to r_{ADP} are comparable with the monomer contribution. At pH > 8.5, the contribution of associates to the kinetics noticeably decreases, and the kinetics is largely determined by the monomeric species [9]. The deviations observed at the initial portion are probably due to the fact that the substitution of OH^- in the dimer and trimers, resulting in the formation of $(DOH^-)H^+$ and analogous trimeric species, does not occur in one step, as was proposed in Schemes 2 and 3,[2] but occurs as a sequence of two steps. H_3O^+ participates in the first of these steps, and OH^- participates in the second. The ratio of the rates of separate steps depends on the pH. In the formation of $(DOH^-)H^+$ and $(DOH^-)H^+ \cdot M \cdot$, coordinated OH^- transfers from the position opposite to γ-P to the position opposite to β-P (Scheme 2). We do not know all the details of the positional changes of OH^- yet, but we do know that the bond between Zn^{2+} and N7 cleaves. Additional experimental data are needed to make the kinetic scheme more complex.

The reaction of OH^- substitution for N7 in the formation of the monomeric $Op(OH^-)_2$ species from $CyOH^-$ and OH^- is characterized by the constant $k_6 = 1.25 \times 10^4$ l mol^{-1} min^{-1} [9]. The value of k_{-14} is 1.2×10^4 l mol^{-1} min^{-1} for the dimer and 4×10^4 l mol^{-1} min^{-1} for the trimer. It is clear that these values are close and they probably characterize the substitution of OH^- for N7 in the coordination sphere of Zn^{2+}. The fact that the $(DOH^-)H^+$ and $(DOH^-)H^+ \cdot M$ species (where M is a monomer Op or Cy) are open conformers is supported by the very close values of $k_8 = 4.5 \times 10^{-3}$ min^{-1} and $k_{15'} = 3 \times 10^{-3}$ min^{-1} that characterize the attack of OH^- on β-P. $k_{15} = 1 \times 10^{-3}$ min^{-1} (for $(DOH^-)H^+$) is the value of the same order of magnitude but somewhat lower. Note that the rate constants k_{10} and $k_{-11} = 1.4 \times 10^4$ l mol^{-1} min^{-1}, which characterize the substitution of OH^- at the Zn^{2+} ion by OH^- at γ-P [9], and the rate constants of the reverse steps (k_{-10} and k_{11}) are of the same order of magnitude as the rate constant of OH^- substitution for N7.

Irrespective of the substitution mechanism description in the formation of $(DOH^-)H^+$ and $(DOH^-)H^+ \cdot M$ (in one step or in a sequence of OH^- substitution reactions), it is clear that OH^- at Zn^{2+} in dimer D and trimers T1 and T2 behaves as a free OH^- ion coordinated to Zn^{2+}. The reaction of substitution by OH^- at Zn^{2+} opposite to β-P can only occur if the coordinated water is ionized at the formation of the dimer. The observation of this substitution provides additional evidence for the main hypothesis that we used in the consideration of the dimer structure determining the pH-independent hydrolysis channel: the coordinated water molecule in D is already ionized, but H^+ has not yet left the reactive dimer and remains in the hydrogen bond. These arguments, together with those published earlier [2, 4, 6, 9, 14], support the fact that proton transfer with the formation of a hydrogen bond is a factor that favors the formation

[2] Earlier, when analyzing the range of high pH, we showed that the addition of the second OH^- does not occur in the pathway of AMP formation, as it does in the formation of the monomeric $Op(OH^-)_2$ species. Schemes 2 and 3, which assume the substitution of OH^- in the reaction center of the dimer and trimers and acceptably describe the kinetics at pH 7.1–7.4, were used in all calculations in [14].

of the attacking nucleophile, and further transformations of intermediates are the consequence of this transfer.

The proven participation of the H_3O^+ ion in the step of the isomeric transformation Op $\rightleftharpoons$ Cy ($ZnATP^{2-}$) (Scheme 2a in [9]) is the most interesting result of this work. We assume that we managed to come near to understanding one of the proton functions in ATP-ases: proton catalyzes the transformation of the inactive ATP conformation into the active one.

ACKNOWLEDGMENTS

This work was supported by the Russian Foundation for Basic Research (grant no. 96-03-32649).

APPENDIX

Parameters of reactions used in kinetic Scheme 3 (variant *21* of the trimeric model) in the calculation of kinetic curves of the ADP and AMP formation in the process of ATP hydrolysis catalyzed by the Zn^{2+} ion

No.	Reaction	Rate constant from Scheme 3	Numerical value
1	$CyOH^- \longrightarrow Cy(ADP) + HPO_4^{2-}$	k_1	$0.007\ min^{-1}$
2	$CyOH^- + OH^- \longrightarrow Op(OH^-)_2$	k_6	$1.25 \times 10^4\ l\ mol^{-1}\ min^{-1}$
3	$Op(OH^-)_2 \longrightarrow CyOH^- + OH^-$	k_{-6}	$0.30\ min^{-1}$
4	$Op(OH^-)_2 \longrightarrow AMP + Zn^{2+} \cdot PP_i$	k_8	$0.0045\ min^{-1}$
5	$OpOH^- + H^+ \longrightarrow Op$	k_{-4}	$6 \times 10^{10}\ l\ mol^{-1}\ min^{-1}$
6	$Op \longrightarrow OpOH^- + H^+$	k_4	$133\ min^{-1}$
7	$CyOH^- + H^+ \longrightarrow Cy$	k_{-3}	$6 \times 10^{10}\ l\ mol^{-1}\ min^{-1}$
8	$Cy \longrightarrow CyOH^- + H^+$	k_3	$50\ min^{-1}$
9	$Op'OH^- \longrightarrow Cy'OH^-$	k_{-7}	$0.0075\ min^{-1}$
10	$Cy'OH^- \longrightarrow Op'OH^-$	k_7	$0.23\ min^{-1}$
11	$D \longrightarrow K(ATP)$	k_{-9}	$0.05\ min^{-1}$
12	$K(ATP) \longrightarrow D$	k_9	$0.13\ min^{-1}$
13	$D \longrightarrow D'$	k_2	$9 \times 10^{-3}\ min^{-1}$
14	$Op'' + H^+ \longrightarrow Cy + H^+$	k_{-5}	$5.8 \times 10^6\ l\ mol^{-1}\ min^{-1}$
15	$Cy + H^+ \longrightarrow Op'' + H^+$	k_5	$2.0 \times 10^6\ l\ mol^{-1}\ min^{-1}$
16	$CyOH^- + OH^- \longrightarrow Cy'OH^- + OH^-$	k_{10}	$1.4 \times 10^4\ l\ mol^{-1}\ min^{-1}$
17	$Cy'OH^- + OH^- \longrightarrow CyOH^- + OH^-$	k_{-10}	$8.0 \times 10^4\ l\ mol^{-1}\ min^{-1}$
18	$OpOH^- + OH^- \longrightarrow Op'OH^- + OH^-$	k_{-11}	$1.4 \times 10^4\ l\ mol^{-1}\ min^{-1}$
19	$Op'OH^- + OH^- \longrightarrow OpOH^- + OH^-$	k_{11}	$8.0 \times 10^4\ l\ mol^{-1}\ min^{-1}$
20	$Op + H^+ \longrightarrow Op' + H^+$	k_{-12}	$1.4 \times 10^8\ l\ mol^{-1}\ min^{-1}$
21	$Op' + H^+ \longrightarrow Op + H^+$	k_{12}	$8.0 \times 10^8\ l\ mol^{-1}\ min^{-1}$
22	$Op' \longrightarrow Op''$	k_{-13}	$10.0\ min^{-1}$
23	$Op'' \longrightarrow Op'$	k_{13}	$10.0\ min^{-1}$
24	$D + OH^- \longrightarrow (DOH^-)H^+ + OH^-$	k_{-14}	$1.2 \times 10^4\ l\ mol^{-1}\ min^{-1}$
25	$(DOH^-)H^+ + OH^- \longrightarrow D + OH^-$	k_{14}	$4.0 \times 10^3\ l\ mol^{-1}\ min^{-1}$

Table (Contd.)

No.	Reaction	Rate constant from Scheme 3	Numerical value
26	$(DOH^-)H^+ \longrightarrow AMP + Cy + Zn^{2+} \cdot PP_i$	k_{15}	1×10^{-3} min^{-1}
27	$D' \longrightarrow D$	k_{-2}	9×10^{-3} min^{-1}
28	$D' \longrightarrow K(ADP) + H_2PO_4^-$	k_{-16}	5 min^{-1}
29	$K(ADP) + H_2PO_4^- \longrightarrow D'$	k_{16}	3.0×10^4 l mol^{-1} min^{-1}
30	$HPO_4^{2-} + H^+ \longrightarrow H_2PO_4^-$	k_{-22}	6.0×10^{10} l mol^{-1} min^{-1}
31	$H_2PO_4^- \longrightarrow HPO_4^{2-} + H^+$	k_{22}	3.79×10^3 min^{-1}
32	$K(ADP) \longrightarrow Cy(ADP) + Cy$	k_{-17}	1.2×10^{10} min^{-1}
33	$Cy(ADP) + Cy \longrightarrow K(ADP)$	k_{17}	6.0×10^{10} l mol^{-1} min^{-1}
34	$Cy(ADP) \longrightarrow CyOH^-(ADP) + H^+$	k_{-18}	384 min^{-1}
35	$CyOH^-(ADP) + H^+ \longrightarrow Cy(ADP)$	k_{18}	6.0×10^{10} l mol^{-1} min^{-1}
36	$CyOH^-(ADP) + OH^- \longrightarrow Op(OH)_2(ADP)$	k_{-19}	1.25×10^4 l mol^{-1} min^{-1}
37	$Op(OH^-)_2(ADP) \longrightarrow CyOH^-(ADP) + OH^-$	k_{19}	0.3 min^{-1}
38	$Cy(ADP) + H^+ \longrightarrow Op(ADP) + H^+$	k_{20}	0.49×10^6 min^{-1}
39	$Op(ADP) + H^+ \longrightarrow Cy(ADP) + H^+$	k_{-20}	1.0×10^6 min^{-1}
40	$Op(ADP) \longrightarrow OpOH^-(ADP) + H^+$	k_{21}	768 min^{-1}
41	$OpOH^-(ADP) + H^+ \longrightarrow Op(ADP)$	k_{-21}	6.0×10^{10} l mol^{-1} min^{-1}
42	$Cy(ADP) + Cy(ADP) \longrightarrow D(ADP)$	k_{-23}	17.0 l mol^{-1} min^{-1}
43	$D(ADP) \longrightarrow Cy(ADP) + Cy(ADP)$	k_{23}	0.1 min^{-1}
44	$Cy + Cy \longrightarrow K(ATP)$	k_{24}	1.5×10^{10} l mol^{-1} min^{-1}
45	$K(ATP) \longrightarrow Cy + Cy$	k_{-24}	1.866×10^8 min^{-1}
46	$K(ATP) + Cy \longrightarrow K_{T1}$	k_{25}	1.5×10^9 l mol^{-1} min^{-1}
47	$K_{Tl} \longrightarrow K(ATP) + Cy$	k_{-25}	2.5×10^8 min^{-1}
48	$K(ATP) + Op \longrightarrow K_{T2}$	k_{25}	1.5×10^9 l mol^{-1} min^{-1}
49	$K_{T2} \longrightarrow K(ATP) + Op$	k_{-25}	2.5×10^8 min^{-1}
50	$K_{T1} \longrightarrow T1$	k_{26}	900 min^{-1}
51	$T1 \longrightarrow K_{T1}$	k_{-26}	10 min^{-1}
52	$K_{T2} \longrightarrow T2$	k_{26}	900 min^{-1}
53	$T2 \longrightarrow K_{T2}$	k_{-26}	10 min^{-1}
54	$T1 \longrightarrow T'1$	$k_{2'}$	2.2×10^{-2} min^{-1}
55	$T'1 \longrightarrow T1$	$k_{-2'}$	2.2×10^{-2} min^{-1}
56	$T2 \longrightarrow T'2$	$k_{2'}$	2.2×10^{-2} min^{-1}
57	$T'2 \longrightarrow T2$	$k_{-2'}$	2.2×10^{-2} min^{-1}

Table (Contd.)

No.	Reaction	Rate constant from Scheme 3	Numerical value
58	T'1 ⟶ D' + Cy	k_{27}	2.5×10^9 min^{-1}
59	D' + Cy ⟶ T'1	k_{-27}	1.5×10^{10} l mol^{-1} min^{-1}
60	T'2 ⟶ D' + Op	k_{27}	2.5×10^9 min^{-1}
61	D' + Op ⟶ T'2	k_{-27}	1.5×10^{10} l mol^{-1} min^{-1}
62	T1 + OH^- ⟶ $(DOH^-)H^+ \cdot$ Cy + OH^-	$k_{-14'}$	4.0×10^4 l mol^{-1} min^{-1}
63	$(DOH^-)H^+ \cdot$ Cy + OH^- ⟶ T1 + OH^-	$k_{14'}$	1.3×10^4 l mol^{-1} min^{-1}
64	T2 + OH^- ⟶ $(DOH^-)H^+ \cdot$ Op+ OH^-	$k_{-14'}$	4.0×10^4 l mol^{-1} min^{-1}
65	$(DOH^-)H^+ \cdot$ Op + OH^- ⟶ T2 + OH^-	$k_{14'}$	1.3×10^4 l mol^{-1} min^{-1}
66	$(DOH^-)H^+ \cdot$ Cy ⟶ AMP + Cy + Cy + $Zn^{2+} \cdot PP_i$	$k_{15'}$	3.0×10^{-3} min^{-1}
67	$(DOH^-)H^+ \cdot$ Op ⟶ AMP + Op + Cy + $Zn^{2+} \cdot PP_i$	$k_{15'}$	3.0×10^{-3} min^{-1}

REFERENCES

1. Utyanskaya, E.Z., Pavlovskii, A.G., Sosfenov, N.I., *et al.*, *Dokl. Akad. Nauk SSSR*, 1988, vol. 301, no. 1, p. 149.
2. Utyanskaya, E.Z., Pavlovskii, A.G., Sosfenov, N.I., *et al.*, *Kinet. Katal.*, 1989, vol. 30, no. 6, p. 1343.
3. Utyanskaya, E.Z. and Shilov, A.E., *Kinet. Katal.*, 1988, vol. 29, no. 1, p. 136.
4. Utyanskaya, E.Z., Pavlov, A.O., Orekhova, E.M., and Lapidus, I.I., *Kinet. Katal.*, 1991, vol. 32, no. 2, p. 349.
5. Utyanskaya, E.Z., Mikhailova, T.V., Pavlov, A.O., *et al.*, *ACH-Models in Chemistry*, 1996, vol. 133, nos. 1–2, p. 65.
6. Utyanskaya, E.Z., Shilov, A.E., Lidskii, B.V., *et al.*, *ACH-Models in Chemistry*, 1996, vol. 133, no. 4, p. 365.
7. Matthies, M. and Zundel, G., *J. Chem, Soc., Perkin Trans. II*, 1977, p. 1824.
8. Takeuchi, H., Murata, H., and Harada, I., *J. Am. Chem. Soc.*, 1988, vol. 110, no. 2, p. 392.
9. Utyanskaya, E.Z., Lidskii, B.V., Neigauz, M.G., and Shilov, A.E., *Kinet. Katal.*, 2000, vol. 41, no. 4, p. 511.
10. Sigel, H., Scheller, K.H., and Milburn, R.M., *Inorg. Chem.*, 1984, vol. 23, no. 13, p. 1933.
11. Tribolet, R., Martin, R., and Sigel, B., *Inorg. Chem.*, 1987, vol. 26, no. 5, p. 638.
12. Sigel, H., *Eur. J. Biochem.*, 1987, vol. 165, no. 1, p. 65.
13. Sigel, H., Tribolet, R., Malini-Balakrishnan, R., *et al.*, *Inorg. Chem.*, 1987, vol. 26, no. 13, p. 2149.
14. Utyanskaya, E.Z., Lidskii, B.V., Neihaus, M.G., and Shilov, A.E., *J. Inorg. Biochem.*, 2000, vol. 81, no. 1, p. 239.
15. Amsler, P. and Sigel, H., *Eur. J. Biochem.*, 1976, vol. 63, no. 3, p. 569.
16. Utyanskaya, E.Z., Pavlov, A.O., Orekhova, E.M., *et al.*, *Zh. Analit. Khim.*, 1990, vol. 45, no. 6, p. 1222.
17. Westheimer, F.H., *Rearrangements in Ground and Excited States*, de Mayo, R., Ed., New York: Academic, 1980; Organic Chemistry, vol. 42-2, p. 229.
18. Kochetkov, S.P., Gabibov, A.G., and Severin, E.S., *Bioorg. Khim.*, 1984, vol. 10, no. 10, p. 1301.
19. Wolcott, R.G. and Boyer, P.D., *Biochem. Biophys. Res. Commun.*, 1974, vol. 57, no. 3, p. 709.
20. Kandpal, R.P., Stempel, K.E., and Boyer, P.D., *Biochemistry*, 1987, vol. 26, no. 6, p. 1512.
21. Syrtsova, L.A., *Usp. Biol. Khim.*, 1989, vol. 30, p. 130.
22. Cross, R.L. and Boyer, P.D., *Biochemistry*, 1975, vol. 14, no. 2, p. 392.
23. Nicholls, D.G., *Bioenergetics: An Introduction to the Chemiosmotic Theory*, London: Academic, 1982, chapter 7.
24. Wang, X., Nelson, D.J., Trindle, C., *et al.*, *J. Inorg. Biochem.*, 1997, vol. 68, no. 1, p. 7.
25. De Meis, L., *FEBS Lett.*, 1987, vol. 213, no. 2, p. 333.
26. Noumi, T., Maeda, M., and Futai, M., *FEBS Lett.*, 1987, vol. 213, no. 2, p. 381.